

Effects of upwelling duration and phytoplankton growth regime on dissolved oxygen levels in an idealized Iberian Peninsula upwelling system

João H. Bettencourt , Vincent Rossi , Lionel Renault , Peter Haynes , Yves Morel ,
Véronique Garçon

Author's reply to Referee #1

We thank the Referee for his/hers comments that helped to greatly improve our manuscript. Below, we provide a point-by-point reply to the referee's comments.

Ref. #1: *There is no mention to the numerical method to integrate the advection-reaction-diffusion Eq(1). Is it Eulerian, semi-Lagrangian, other? What about numerical diffusion, is it relevant?*

Authors : *Eq (1) is solved online by the ROMS model itself, i. e., concurrently with the hydrodynamic equations, following an Eulerian approach. The model splits the advective part in horizontal advection that is solved by a 3rd order upstream method and vertical advection that uses a 4th order centered method. The horizontal diffusive operator is harmonic and the reaction term is solved by an iterative method, with three fractional time steps to achieve implicit discretization of the biological interactions. The 1D model is solved in the same manner as we used the 1D version of ROMS to perform the simulations. Since the numerical schemes chosen to solve the equations are known to be over diffusive, we did not include explicit diffusion in the model; hence, numerical diffusion is the only source of diffusion in the simulations.*

Ref. #1: *Contrasting with this, Appendix A was very detailed. Is it necessary to include so many details to obtain a numerical fixed point when standard softwares (mathematica, matlab,...) makes the work easily? In any case I found this Appendix difficult to follow and I would ask the authors to smooth it out.*

Authors: *We have dropped the details of the fixed point search and we have considerably shortened Appendix A to make it easier to follow.*

Ref. #1: *I think it can be helpful for the discussion if you show the full set of advection-reaction- diffusion equations with all the terms and not in different pieces (Eq (3-4), and all the discussion below). In particular, the way the authors address the air-sea exchange flux term was unclear for me.*

Authors: *We have improved the way we present the model equations in the new version of the manuscript. All terms pertaining to dissolved O₂, P and Z are now shown as one fully-developed differential equation for each species:*

“In the coupled model, the time evolution of DO, P and Z concentrations are given by, respectively:

$$\frac{\partial [O_2]}{\partial t} + u\frac{\partial [O_2]}{\partial x} + v\frac{\partial [O_2]}{\partial y} + w\frac{\partial [O_2]}{\partial z} = k_H (\frac{\partial^2 [O_2]}{\partial x^2} + \frac{\partial^2 [O_2]}{\partial y^2}) + \frac{\partial}{\partial z}(\langle [O_2] 'w' \rangle - k_V \frac{\partial [O_2]}{\partial z}) + V_a ([O_2] - [O_2]_{sat}) + A_J(z)f([O_2])[P] - u_r([O_2],[P]) - v_r([O_2],[Z]) - m[O_2], \quad (1)$$

Effects of upwelling duration and phytoplankton growth regime on dissolved oxygen levels in an idealized Iberian Peninsula upwelling system

João H. Bettencourt , Vincent Rossi , Lionel Renault , Peter Haynes , Yves Morel ,
Véronique Garçon

List of relevant changes

Deletions:

Marine hypoxia is an increasing global concern that is exacerbated by climate change, directly through warming-induced increase of stratification and decrease of oxygen solubility, and indirectly by changes in circulation and wind forcing (Levin, 2018).

Upwelling systems are thus especially sensitive to deoxygenation (Paulmier and Ruiz-Pino, 2009) and to episodic hypoxia events with deleterious effects on marine life and human activities such as fisheries (Grantham et al., 2004; Hales et al., 2006; McClatchie et al. 2010; Roegner et al., 2011).

Moreover, diatoms growth is thought to be positively correlated with the upwelling-driven nitrate inputs; in contrast, the growth of other planktonic groups can be insensitive to and even limited by newly-upwelled nitrates, especially when colimitation prevails or in the absence of necessary micro-nutrients.

On top of the oxygen that is produced and consumed within marine ecosystems, a considerable part of dissolved oxygen eventually become gaseous and is then exchanged at the ocean-atmosphere interface, contributing to the estimations that more than one half of atmospheric oxygen is produced in the ocean (Harris, 1986).

In the coupled model, the time evolution of a tracer concentration C is given by:

$$\frac{\partial C}{\partial t} + u\frac{\partial C}{\partial x} + v\frac{\partial C}{\partial y} + w\frac{\partial C}{\partial z} = k(\frac{\partial^2 C}{\partial x^2} + \frac{\partial^2 C}{\partial y^2} + \frac{\partial^2 C}{\partial z^2}) + F_A + Q_C \quad (1)$$

where (u, v, w) is the 3D velocity field, k the tracer diffusivity, F_A is the air-sea oxygen exchange flux term (positive when the ocean receives oxygen) and Q_C is the source/sink term for the tracer C , here defined by the biogeochemical model O₂PZ (SP2015). It simulates seven biogeochemical reactions between the three compartments (Fig. 2) as follows:

$$Q_{O_2} = A J(z) f([O_2])[P] - u_r([O_2], [P]) - v_r([O_2], [Z]) - m[O_2] \quad (2)$$

$$Q_P = l(N) g([O_2], [P]) - e([P], [Z]) - \sigma[P] \quad (3)$$

$$Q_Z = \kappa([O_2]) e([P], [Z]) - \mu[Z] \quad (4)$$

In the source/sink term expression for DO (Eq. 2),

We compared the full ranges of densities ρ , DO concentrations $[O_2]$, and chlorophyll-a concentrations $[Chl-a]$ of the reference simulation to all compiled measurements collected during the MOUTON campaign. We confirm that the coupled model, although of low complexity, reproduces relatively well the ρ - $[O_2]$ and ρ - $[Chl-a]$ relationships obtained from in-situ observations, despite a slight underestimation of $[O_2]$ and $[Chl-a]$ (Fig. 4). Note however that the cruise was specially designed to sample high coastal chlorophyll concentrations observed from satellite, so the dataset used in the comparison is biased towards high chlorophyll conditions.

Similarly, Gutknecht *et al.* (2013) in their modelling study of the Benguela upwelling region found a low $[O_2]$ plume for the climatological month of December at the shelf edge. For the Oregon coast, Hales *et al.* (2006) measured $[O_2]$ of 70-110 mmol m⁻³ in upwelled water at the shelf break, about 200 mmol m⁻³ less than at the surface, which is the same range of the vertical gradient simulated here.

validate

well

To proceed, we consider first the system obtained by setting $[Z] = 0$.

Applying the fixed point condition (A1), we obtain two equations relating $[P]$ and $[O_2]$:

$$P_1([O_2]) = (m[O_2]([O_2+c_0])([O_2]+c_2))/(Ac_0c_2+(A-\delta)c_0[O_2]-\delta[O_2]^2) \quad (A2)$$

$$P_2([O_2]) = 1/\gamma(Bc/([O_2]+c_1) - \sigma) \quad (A3)$$

The fixed points of the system are given by $P_1 = P_2$ in the positive quadrant of the $([O_2], [P]; [Z] = 0)$ plane, in addition to the extinction steady state. Explicit computation of the fixed points is not possible for the $[O_2]$ - $[P]$ - $[Z]$ system, but we can derive relationships of the form $[Z] = f([O_2], [P])$ that satisfy (A1) from the oxygen and phytoplankton equations, as follows:

$$Z_1([O_2], [P]) = ([O_2] + c_3)/\nu[O_2] ((Ac_0[P])/([O_2]+c_0)-(\delta[O_2][P])/([O_2]+c_2)-m[O_2]) \quad (A4)$$

$$Z_2([O_2], [P]) = ([P]+h)/\beta[P] (B[O_2][P]/([O_2]+c_1)-\gamma[P]^2-\sigma[P]) \quad (A5)$$

The zooplankton equation does not produce a similar relationship. Instead, analytical manipulation of it let us derive the following expression:

$$[Z]=0 \vee [P]=P_z=hM([O_2])/(1-M([O_2])), \quad (A6)$$

where $M([O_2])=\mu/\beta ([O_2]^2+c_4^2)/\eta[O_2]^2$. The fixed points of the $[O_2]$ - $[P]$ - $[Z]$ system are the locii of intersection of Eqs. (A4)-(A6) in the $([O_2] > 0; [P] > 0; [Z] > 0)$ octant. Note that the terms in parenthesis in Eqs. (A4), (A5) are the equations of the oxygen-phytoplankton system. In fact, if $[Z] = 0$, Eqs. (A4), (A5) reduce to Eqs. (A2), (A3), as expected.

Since the position of the fixed points of the system is given by the intersections of the isoclines Z_1 , Z_2 and P_z , they should intersect at or near $([O_2]^w, [P]^w)$ and the fixed point at the intersection should be stable. This can be achieved by changing the parameters of the system in order to move the isoclines in phase-space, and at the same time check the sign of the real part of the eigenvalues of the system Jacobian matrix at the intersection to identify the stability type of the fixed point. In Fig. A1, we plot the three isoclines in the plane $\nu = 0$ for different values of the parameters A , B and h . It shows how the isoclines change with the changing parameters. Since both Z_1 and Z_2 depend on $[Z]$, we must look at the 3D phase space to see where the isoclines intersect (Fig. A2).

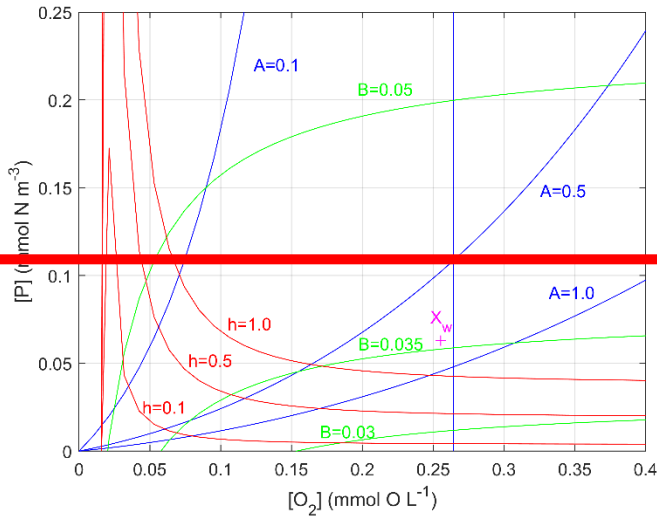


Figure A1. Isoclines of the $[O_2]$ - $[P]$ system for selected values of A , B and h . Blue: P_1 ; Green: P_2 ; Red: P_z .

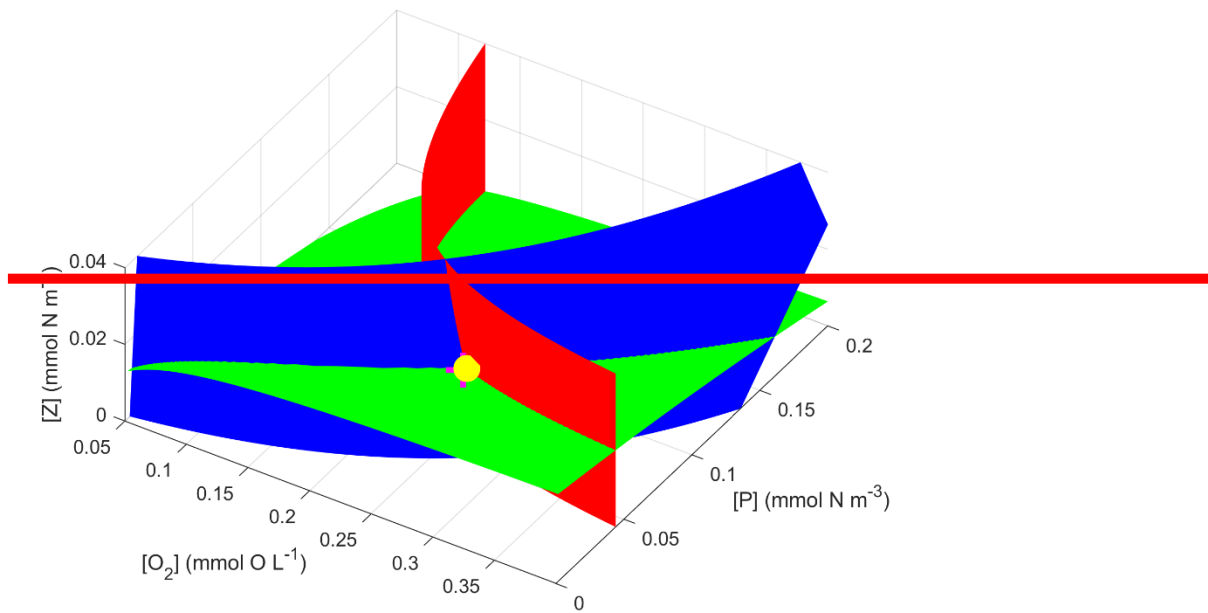


Figure A2. Isoclines of the $[O_2]$ - $[P]$ - $[Z]$ system. Blue: Z_1 ; Green: Z_2 ; Red: P_z . Yellow: X^0 . To build this figure, we set up a grid of $([O_2]_i; [P]_j)$; $i, j = 1; \dots; N$ values and plotted $Z_1(i; j)$ and $Z_2(i; j)$ from Eqs. (A4) and (A5). The P_z isocline is different since it does not depend on $[Z]$, so we computed $P_z(i) = hM(c_i) / (1 - M(c_i))$ with M defined in the text, and extended it vertically up.

To find the intersection point, that corresponds to the co-existence steady state X^0 , we computed the distance $d_{12}(i; j) = Z_2(i; j) - Z_1(i; j)$, so that the intersection $Z_2 = Z_1$ is given by $d_{12} = 0$. The zeros of d_{12} were identified approximately by choosing, for each $[O_2]_i$, the value of $[P]_j$ that minimized $d_{12}(i; j)$. To find X^0 , we used a similar procedure to find the point where this line intersects P_z . This procedure is approximate, and its accuracy varies with N . By performing tests for several N , we found that $N = 300$ gave enough accuracy. By varying A , B and h , the intersection (X^0) can be made to approach X^w . Although other parameters may be varied instead of these three, we found that these are the ones whose variations are easier to judge in terms of displacement of the isoclines. We note that, of the three, only h is one of the "fixed" parameters that was found in the literature, but since it is quite easy to move P_z by changing its value, we decided to use it as a tuning parameter. The result of this exercise is that the

Levin, L. A.: Manifestation, Drivers, and Emergence of Open Ocean Deoxygenation, Annual Review of Marine Science, doi:10.1146/annurev-marine-121916-063359, 2018.

Insertions:

Upwelling systems are thus especially sensitive to episodic and long-term changes in DO levels with deleterious effects on marine life and human activities such as fisheries (Grantham et al., 2004; Hales et al., 2006; Paulmier and Ruiz-Pino, 2009; McClatchie et al. 2010; Roegner et al., 2011).

DO levels in these subsurface waters are thought to diminish during the upwelling season due to strong remineralization of sinking organic matter as well as to mixing with poorly-ventilated waters of subtropical origins (Castro et al., 2006). Overall, DO appears to partly control the remineralization of dissolved organic carbon in the IPUS and more generally in key water masses of the North Atlantic (Alvarez-Salgado et al. 2013).

In the Iberian basin, the Eastern North Atlantic Central Water (ENACW) mass of subtropical origin, whose archetypal concentrations of DO are initially low, would be ventilated by eddy-induced mixing with more oxygenated ENACW of subpolar origin (Pèrez et al., 2001).

Moreover, diatoms growth is thought to be positively correlated with the upwelling-driven nitrate inputs (Sarhou et al., 2005); in contrast, the growth of other planktonic groups can be insensitive to and even

limited by newly-upwelled nitrates (Mahaffey, 2005), especially when colimitation prevails or in the absence of necessary micro-nutrients.

The low-complexity O₂PZ model was directly implemented into the CROCO model following one of the already-embedded biogeochemical modules; it allows maintaining the full capabilities and versatility of this community code while gaining in computing efficiency (allowing extensive sensitivity studies and the consideration of submesoscale dynamics in oxygen cycling) as compared to the more complex biogeochemical modules already available within CROCO.

In the coupled model, the time evolution of DO, P and Z concentrations are given by, respectively:

$$\begin{aligned} \frac{\partial [O_2]}{\partial t} + u\frac{\partial [O_2]}{\partial x} + v\frac{\partial [O_2]}{\partial y} + w\frac{\partial [O_2]}{\partial z} = k_H (\frac{\partial^2 [O_2]}{\partial x^2} + \frac{\partial^2 [O_2]}{\partial y^2}) + \frac{\partial}{\partial z}(\langle [O_2] 'w' \rangle - k_V \frac{\partial [O_2]}{\partial z}) + Va ([O_2] - [O_2]_{sat}) + AJ(z)f([O_2])[P] - u_r([O_2],[P]) - v_r([O_2],[Z]) - m[O_2], \end{aligned} \quad (1)$$

$$\frac{\partial [P]}{\partial t} + u\frac{\partial [P]}{\partial x} + v\frac{\partial [P]}{\partial y} + w\frac{\partial [P]}{\partial z} = k_H (\frac{\partial^2 [P]}{\partial x^2} + \frac{\partial^2 [P]}{\partial y^2}) + \frac{\partial}{\partial z}(\langle [P] 'w' \rangle - k_V \frac{\partial [P]}{\partial z}) + l(N)g([O_2],[P]) - e([P],[Z]) - \sigma[P], \quad (2)$$

$$\frac{\partial [Z]}{\partial t} + u\frac{\partial [Z]}{\partial x} + v\frac{\partial [Z]}{\partial y} + w\frac{\partial [Z]}{\partial z} = k_H (\frac{\partial^2 [Z]}{\partial x^2} + \frac{\partial^2 [Z]}{\partial y^2}) + \frac{\partial}{\partial z}(\langle [Z] 'w' \rangle - k_V \frac{\partial [Z]}{\partial z}) + \kappa([O_2])e([P],[Z]) - \mu[Z], \quad (3)$$

where (u, v, w) is the 3D velocity field, k_H and k_V are the horizontal and vertical tracer diffusivities, and $\langle \dots \rangle$ are the vertical turbulent fluxes. The biogeochemical model O₂PZ (SP2015) defines the source terms of DO, P and Z in the coupled model. It simulates seven biogeochemical reactions between the three compartments (Fig. 2) as follows: in the DO equation (Eq. 1),

On top of the oxygen that is produced and consumed within marine ecosystems, a considerable part of dissolved oxygen eventually becomes gaseous and is then exchanged at the ocean-atmosphere interface, contributing to the estimations that more than one half of atmospheric oxygen is produced in the ocean (Harris, 1986). The remaining term of Eq. (2) is the air-sea flux of O₂, which is the product of the gas transfer velocity Va , that depends on the square of the wind speed and on the Schmidt number (Wanninkhof, 1992), with the difference of the oceanic DO concentration and the solubility of O₂ in seawater.

This term is included here to circumvent the absence of nutrient limitation in the original O₂PZ model of SP2015. We chose to add a parametrization instead of a new equation for the nutrients because this last option would necessarily increase the complexity of the model.

The cross-shore wind component is zero in all cases. Despite the fact that “true” wind patterns observed over Western Iberia are undoubtedly more variable (both in terms of direction and magnitude) than our idealized forcing inspired from a specific campaign, it provides the quickest development of a clear upwelling front generating small-scale instabilities. Note that sensitivity tests were performed (not shown) and revealed that the model responses are qualitatively similar among different wind strengths, given that the magnitude is high enough to ensure the development of the unstable upwelling front.

We compared the full ranges of densities ρ , DO concentrations $[O_2]$, and chlorophyll-a concentrations $[Chl-a]$ of the reference simulation to all compiled measurements collected during the MOUTON campaign. Given the low-complexity of the biogeochemical model and the highly idealized physical setting, a fully quantitative comparison is out of scope, however we confirm that the coupled model reproduces qualitatively well the ρ - $[O_2]$ and ρ - $[Chl-a]$ relationships obtained from in-situ observations.

In a qualitative sense our idealized model results are similar to more realistic model studies such as Gutknecht *et al.* (2013) which in their modelling study of the Benguela upwelling region found a low $[O_2]$ plume for the climatological month of December at the shelf edge, and to observational studies such as Hales *et al.* (2006), which for the Oregon coast, measured $[O_2]$ of 70-110 mmol m⁻³ in upwelled water at the shelf break, about 200 mmol m⁻³ less than at the surface, which is the same range of the vertical gradient simulated here.

The low-complexity O₂PZ model accounts for oxygen production by photosynthesis and consumption by both respiration and remineralization but its simplicity does not allow to include other oceanographic

processes that could influence oxygen cycling over shallow shelves, such as for instance the complex benthic-pelagic coupled processes (Capet et al., 2016).

compare

qualitatively

In permanent Oxygen Minimum Zones (OMZs), changes in physical forcing (e.g. wind regime) and/or biological characteristics (e.g. size structure or functional types) can have dire implications for marine ecosystems and fisheries management. Indeed, the measured expansion of the Tropical Atlantic and Pacific OMZs (Stramma et al., 2008) implies a shallower upper boundary of the low O₂ core and an increased sensitivity of oxygen levels over the continental shelf to upwelling winds, which are indeed predicted to intensify with climate change (Sydeman et al., 2014). Future work could be focused on understanding this high sensitivity and on anticipating how it would affect the stability of the coupled-system in a changing climate.

This results in a

that

Álvarez-Salgado, X.A., Nieto-Cid, M., Álvarez, M., Pérez, F.F., Morin, P., Mercier, H.: New insights on the mineralization of dissolved organic matter in central, intermediate, and deep water masses of the northeast North Atlantic. *Limnol. Oceanogr.* 58, 681–696. doi.org/10.4319/lo.2013.58.2.0681, 2013.

Capet, A., Meysman, F.J.R., Akoumianaki, I., Soetaert, K., Grégoire, M.: Integrating sediment biogeochemistry into 3D oceanic models: A study of benthic-pelagic coupling in the Black Sea. *Ocean Modelling* 101, 83–100. doi.org/10.1016/j.ocemod.2016.03.006, 2016.

Castro, C.G., Nieto-Cid, M., Álvarez-Salgado, X.A., Pérez, F.F.: Local remineralization patterns in the mesopelagic zone of the Eastern North Atlantic, off the NW Iberian Peninsula. *Deep Sea Research Part I: Oceanographic Research Papers* 53, 1925–1940. doi.org/10.1016/j.dsr.2006.09.002, 2006.

Laffoley, D. and Baxter, J., 2019, *Ocean deoxygenation : everyone's problem : causes, impacts, consequences and solutions*, IUCN Report, Gland, Switzerland, 562 pages, doi.org/10.2305/IUCN.CH.2019.13.en

Pérez, F.F., Castro, C.G., Álvarez-Salgado, X.A., Ríos, A.F.: Coupling between the Iberian basin — scale circulation and the Portugal boundary current system: a chemical study. *Deep Sea Research Part I: Oceanographic Research Papers* 48, 1519–1533. doi.org/10.1016/S0967-0637(00)00101-1, 2001.

Sarthou, G., Timmermans, K.R., Blain, S., Tréguer, P.: Growth physiology and fate of diatoms in the ocean: a review. *Journal of Sea Research, Iron Resources and Oceanic Nutrients - Advancement of Global Environmental Simulations* 53, 25–42. doi.org/10.1016/j.seares.2004.01.007, 2005.

Stramma, L., Johnson, G.C., Sprintall, J., Mohrholz, V.: Expanding Oxygen-Minimum Zones in the Tropical Oceans. *Science* 320, 655–658. doi.org/10.1126/science.1153847, 2008.

Sydeman, W.J., García-Reyes, M., Schoeman, D.S., Rykaczewski, R.R., Thompson, S.A., Black, B.A., Bograd, S.J.: Climate change and wind intensification in coastal upwelling ecosystems. *Science* 345, 77–80. doi.org/10.1126/science.1251635, 2014.

Wanninkhof, R.: Relationship between wind speed and gas exchange over the ocean, *Journal of Geophysical Research*, 97(C5), 7373, doi:10.1029/92JC00188, 1992.

$$\partial[P]/\partial t + u\partial[P]/\partial x + v\partial[P]/\partial y + w\partial[P]/\partial z = k_H (\partial^2[P]/\partial x^2 + \partial^2[P]/\partial y^2) + \partial/\partial z(\langle [P]'w' \rangle - k_V \partial[P]/\partial z) + l(N)g([O_2],[P]) - e([P],[Z]) - \sigma[P], \quad (2)$$

$$\partial[Z]/\partial t + u\partial[Z]/\partial x + v\partial[Z]/\partial y + w\partial[Z]/\partial z = k_H (\partial^2[Z]/\partial x^2 + \partial^2[Z]/\partial y^2) + \partial/\partial z(\langle [Z]'w' \rangle - k_V \partial[Z]/\partial z) + \kappa([O_2])e([P],[Z]) - \mu[Z], \quad (3)$$

where (u,v,w) is the 3D velocity field, k_H and k_V are the horizontal and vertical tracer diffusivities, and $\langle \dots \rangle$ are the vertical turbulent fluxes.”

We have also rewritten the text and developed our explanations to better describe the Air-Sea exchange term:

“On top of the oxygen that is produced and consumed within marine ecosystems, a considerable part of dissolved oxygen eventually becomes gaseous and is then exchanged at the ocean-atmosphere interface, contributing to the estimations that more than one half of atmospheric oxygen is produced in the ocean (Harris, 1986). The remaining term of Eq. (2) is the air-sea flux of O_2 , which is the product of the gas transfer velocity V_a , that depends on the square of the wind speed and on the Schmidt number (Wanninkhof, 1992), with the difference of the oceanic DO concentration and the solubility of O_2 in seawater.”

Ref. #1: *After reading several times, I do not understand Fig. 6e. Please clarify its meaning. Is it really helpful?*

Authors : *Figure 6e displays the alongshore averaged concentrations of O_2 for each binned value of the Okubo-Weiss criterion (γ). It is computed from the data of figure 6d by averaging the values in the map “horizontally”, that is along the x -axis for a constant γ level. It emphasizes the result that, on average, there are higher O_2 concentrations in the rotation-dominated regions ($\gamma < 0$) as compared against strain-dominated regions ($\gamma > 0$); this information is not readily observable in figure 6d.*

Ref. #1: *In the discussion/conclusions section I missed some discussion on the relevance of the results of this work on permanent marine oxygen minimum zones*

Authors : *Thank you for this pertinent suggestion; we have added a few words about this topic in the discussion section:*

“In permanent Oxygen Minimum Zones (OMZs), changes in physical forcing (e.g. wind regime) and/or biological characteristics (e.g. size structure or functional types) can have dire implications for marine ecosystems and fisheries management. Indeed, the measured expansion of the Tropical Atlantic and Pacific OMZs (Stramma et al., 2008) implies a shallower upper boundary of the low O_2 core and an increased sensitivity of oxygen levels over the continental shelf to upwelling winds, which are indeed predicted to intensify with climate change (Sydeman et al., 2014). Future work could be focused on understanding this high sensitivity and on anticipating how it would affect the stability of the coupled-system in a changing climate.”

Authors’ reply to Referee #2

We thank the Referee for his/her comments that helped to greatly improve our manuscript. Below, we provide a point-by-point reply to all referee’s comments.

Ref. #2: *While I generally agree with the comments of Referee #1, in terms of the quality of the manuscript, and its relevance of publication, there are a number of points that I will refer to, which should be addressed before the final publication. On the one hand, the configuration used is highly idealized, and the practical application to the Iberian system is not straightforward. Provided the simplifications that were done related the idealized configuration, and the theoretical approach, (quite difficult to read to oceanographers not specialized in theoretical oceanography) I have some doubts about the practical applicability of the results, and the interest that it may have for the oceanographic community of the region, devoted to the study of biogeochemical processes, (constituted mainly by chemical oceanographers).*

Authors: *We acknowledge the concerns of Referee 2 concerning the future applicability of our results due to the theoretical character of our study. This contribution is indeed, to our knowledge, the first and unique attempt to develop a low complexity ocean coupled model (“NPZD-type”, which has been proven very useful for the Oceanographic community) centered on oxygen by building upon recent mathematical modelling. To strengthen the utility and the potential applicability of our results, we have rewritten several parts of the manuscript (shown below in the replies) to better summarize our results and make it easier for the oceanographic community to follow the theoretical description of our model (please check the revised appendix A).*

Ref. #2: *1 - Introduction: Paragraph 1. The Iberian region is not an example of a region of marine hypoxia, and that should be referred to in the manuscript. References to de-oxygenation (line 40) do not make much sense in the scope of this manuscript.*

Authors: *Following your recommendations, we have modified the Introduction section by removing the references to marine hypoxia and deoxygenation and by introducing additional references as suggested by the next comment. Both first paragraphs of the Introduction have been rewritten accordingly:*

“Declining dissolved oxygen (DO) in the world ocean and coastal realm impacts all marine life, from microbes to higher trophic levels (Breitburg et al., 2018), with consequences ranging from ecological adaptations and shifts (Gilly et al., 2013), changes of biogeochemical activity (Wright et al., 2012) to mass mortality events (Diaz and Rosenberg, 2008) and biodiversity restructuring (Vaquer-Sunyer and Duarte, 2008).

Coastal waters are generally eutrophic and characterized by substantial planktonic productivity at the surface which favours oxygen consumption through remineralization of sinking organic matter, leading to low levels of DO in subsurface and near-bottom waters. Highly productive surface waters are typical of coastal upwelling regions and sustain socio-economically important ecosystems. **Upwelling systems are thus especially sensitive to episodic and long-term changes in DO levels with deleterious effects on marine life and human activities such as fisheries (Grantham et al., 2004; Hales et al., 2006; Paulmier and Ruiz-Pino, 2009; McClatchie et al. 2010; Roegner et al., 2011).**”

Ref. #2: *2 - The authors barely refer to the observational literature related to the oxygen cycle in the Iberian region, limiting themselves to cite Rossi’s articles (2010, 2013), which consist of a single campaign, not particularly devoted to that subject. There is some observational literature including the oxygen cycle that I think should be cited, as it is relevant. (Hint: Alvarez-Salgado, X.A, Perez, F.F, Castro, C.G. , all of them in IIM-CSIC-Vigo, Spain) On the other hand there are oceanographic processes not solved by the model that*

Effects of upwelling duration and phytoplankton growth regime on dissolved oxygen levels in an idealized Iberian Peninsula upwelling system

João H. Bettencourt , Vincent Rossi , Lionel Renault , Peter Haynes , Yves Morel ,
Véronique Garçon

List of relevant changes

Deletions:

Marine hypoxia is an increasing global concern that is exacerbated by climate change, directly through warming-induced increase of stratification and decrease of oxygen solubility, and indirectly by changes in circulation and wind forcing (Levin, 2018).

Upwelling systems are thus especially sensitive to deoxygenation (Paulmier and Ruiz-Pino, 2009) and to episodic hypoxia events with deleterious effects on marine life and human activities such as fisheries (Grantham et al., 2004; Hales et al., 2006; McClatchie et al. 2010; Roegner et al., 2011).

Moreover, diatoms growth is thought to be positively correlated with the upwelling-driven nitrate inputs; in contrast, the growth of other planktonic groups can be insensitive to and even limited by newly-upwelled nitrates, especially when colimitation prevails or in the absence of necessary micro-nutrients.

On top of the oxygen that is produced and consumed within marine ecosystems, a considerable part of dissolved oxygen eventually become gaseous and is then exchanged at the ocean-atmosphere interface, contributing to the estimations that more than one half of atmospheric oxygen is produced in the ocean (Harris, 1986).

In the coupled model, the time evolution of a tracer concentration C is given by:

$$\frac{\partial C}{\partial t} + u\frac{\partial C}{\partial x} + v\frac{\partial C}{\partial y} + w\frac{\partial C}{\partial z} = k(\frac{\partial^2 C}{\partial x^2} + \frac{\partial^2 C}{\partial y^2} + \frac{\partial^2 C}{\partial z^2}) + F_A + Q_C \quad (1)$$

where (u, v, w) is the 3D velocity field, k the tracer diffusivity, F_A is the air-sea oxygen exchange flux term (positive when the ocean receives oxygen) and Q_C is the source/sink term for the tracer C , here defined by the biogeochemical model O₂PZ (SP2015). It simulates seven biogeochemical reactions between the three compartments (Fig. 2) as follows:

$$Q_{O_2} = A J(z) f([O_2])[P] - u_r([O_2], [P]) - v_r([O_2], [Z]) - m[O_2] \quad (2)$$

$$Q_P = l(N) g([O_2], [P]) - e([P], [Z]) - \sigma[P] \quad (3)$$

$$Q_Z = \kappa([O_2]) e([P], [Z]) - \mu[Z] \quad (4)$$

In the source/sink term expression for DO (Eq. 2),

We compared the full ranges of densities ρ , DO concentrations $[O_2]$, and chlorophyll-a concentrations $[Chl-a]$ of the reference simulation to all compiled measurements collected during the MOUTON campaign. We confirm that the coupled model, although of low complexity, reproduces relatively well the ρ - $[O_2]$ and ρ - $[Chl-a]$ relationships obtained from in-situ observations, despite a slight underestimation of $[O_2]$ and $[Chl-a]$ (Fig. 4). Note however that the cruise was specially designed to sample high coastal chlorophyll concentrations observed from satellite, so the dataset used in the comparison is biased towards high chlorophyll conditions.

Similarly, Gutknecht *et al.* (2013) in their modelling study of the Benguela upwelling region found a low $[O_2]$ plume for the climatological month of December at the shelf edge. For the Oregon coast, Hales *et al.* (2006) measured $[O_2]$ of 70-110 mmol m⁻³ in upwelled water at the shelf break, about 200 mmol m⁻³ less than at the surface, which is the same range of the vertical gradient simulated here.

validate

well

To proceed, we consider first the system obtained by setting $[Z] = 0$.

Applying the fixed point condition (A1), we obtain two equations relating $[P]$ and $[O_2]$:

$$P_1([O_2]) = (m[O_2]([O_2+c_0])([O_2]+c_2))/(Ac_0c_2+(A-\delta)c_0[O_2]-\delta[O_2]^2) \quad (A2)$$

$$P_2([O_2]) = 1/\gamma(Bc/([O_2]+c_1) - \sigma) \quad (A3)$$

The fixed points of the system are given by $P_1 = P_2$ in the positive quadrant of the $([O_2], [P]; [Z] = 0)$ plane, in addition to the extinction steady state. Explicit computation of the fixed points is not possible for the $[O_2]$ - $[P]$ - $[Z]$ system, but we can derive relationships of the form $[Z] = f([O_2], [P])$ that satisfy (A1) from the oxygen and phytoplankton equations, as follows:

$$Z_1([O_2], [P]) = ([O_2] + c_3)/\nu[O_2] ((Ac_0[P])/([O_2]+c_0)-(\delta[O_2][P])/([O_2]+c_2)-m[O_2]) \quad (A4)$$

$$Z_2([O_2], [P]) = ([P]+h)/\beta[P] (B[O_2][P]/([O_2]+c_1)-\gamma[P]^2-\sigma[P]) \quad (A5)$$

The zooplankton equation does not produce a similar relationship. Instead, analytical manipulation of it let us derive the following expression:

$$[Z]=0 \vee [P]=P_z=hM([O_2])/(1-M([O_2])), \quad (A6)$$

where $M([O_2])=\mu/\beta ([O_2]^2+c_4^2)/\eta[O_2]^2$. The fixed points of the $[O_2]$ - $[P]$ - $[Z]$ system are the locii of intersection of Eqs. (A4)-(A6) in the $([O_2] > 0; [P] > 0; [Z] > 0)$ octant. Note that the terms in parenthesis in Eqs. (A4), (A5) are the equations of the oxygen-phytoplankton system. In fact, if $[Z] = 0$, Eqs. (A4), (A5) reduce to Eqs. (A2), (A3), as expected.

Since the position of the fixed points of the system is given by the intersections of the isoclines Z_1 , Z_2 and P_z , they should intersect at or near $([O_2]^w, [P]^w)$ and the fixed point at the intersection should be stable. This can be achieved by changing the parameters of the system in order to move the isoclines in phase-space, and at the same time check the sign of the real part of the eigenvalues of the system Jacobian matrix at the intersection to identify the stability type of the fixed point. In Fig. A1, we plot the three isoclines in the plane $\nu = 0$ for different values of the parameters A , B and h . It shows how the isoclines change with the changing parameters. Since both Z_1 and Z_2 depend on $[Z]$, we must look at the 3D phase space to see where the isoclines intersect (Fig. A2).

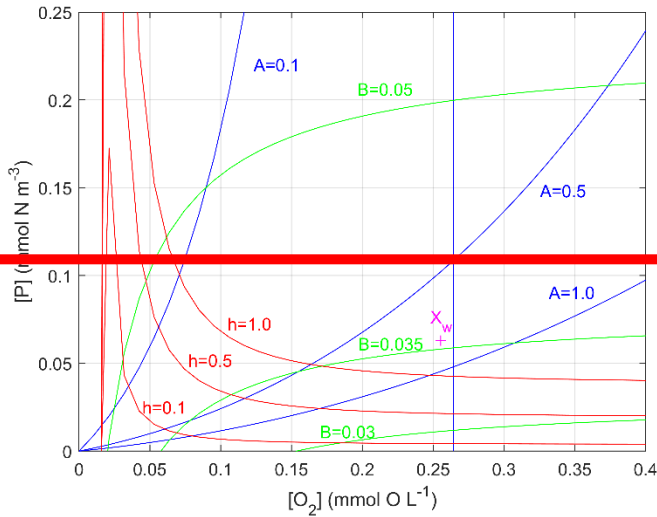


Figure A1. Isoclines of the $[O_2]$ - $[P]$ system for selected values of A , B and h . Blue: P_1 ; Green: P_2 ; Red: P_z .

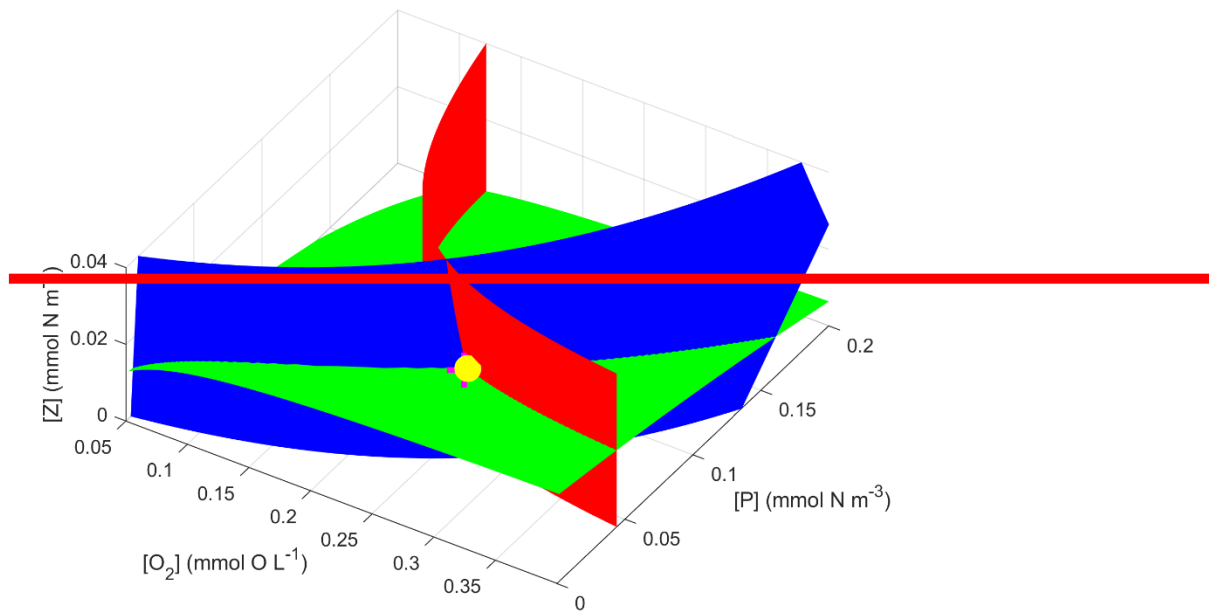


Figure A2. Isoclines of the $[O_2]$ - $[P]$ - $[Z]$ system. Blue: Z_1 ; Green: Z_2 ; Red: P_z . Yellow: X^0 . To build this figure, we set up a grid of $([O_2]_i; [P]_j)$; $i, j = 1; \dots; N$ values and plotted $Z_1(i; j)$ and $Z_2(i; j)$ from Eqs. (A4) and (A5). The P_z isocline is different since it does not depend on $[Z]$, so we computed $P_z(i) = hM(c_i) / (1 - M(c_i))$ with M defined in the text, and extended it vertically up.

To find the intersection point, that corresponds to the co-existence steady state X^0 , we computed the distance $d_{12}(i; j) = Z_2(i; j) - Z_1(i; j)$, so that the intersection $Z_2 = Z_1$ is given by $d_{12} = 0$. The zeros of d_{12} were identified approximately by choosing, for each $[O_2]_i$, the value of $[P]_j$ that minimized $d_{12}(i; j)$. To find X^0 , we used a similar procedure to find the point where this line intersects P_z . This procedure is approximate, and its accuracy varies with N . By performing tests for several N , we found that $N = 300$ gave enough accuracy. By varying A , B and h , the intersection (X^0) can be made to approach X^w . Although other parameters may be varied instead of these three, we found that these are the ones whose variations are easier to judge in terms of displacement of the isoclines. We note that, of the three, only h is one of the "fixed" parameters that was found in the literature, but since it is quite easy to move P_z by changing its value, we decided to use it as a tuning parameter. The result of this exercise is that the

Levin, L. A.: Manifestation, Drivers, and Emergence of Open Ocean Deoxygenation, Annual Review of Marine Science, doi:10.1146/annurev-marine-121916-063359, 2018.

Insertions:

Upwelling systems are thus especially sensitive to episodic and long-term changes in DO levels with deleterious effects on marine life and human activities such as fisheries (Grantham et al., 2004; Hales et al., 2006; Paulmier and Ruiz-Pino, 2009; McClatchie et al. 2010; Roegner et al., 2011).

DO levels in these subsurface waters are thought to diminish during the upwelling season due to strong remineralization of sinking organic matter as well as to mixing with poorly-ventilated waters of subtropical origins (Castro et al., 2006). Overall, DO appears to partly control the remineralization of dissolved organic carbon in the IPUS and more generally in key water masses of the North Atlantic (Alvarez-Salgado et al. 2013).

In the Iberian basin, the Eastern North Atlantic Central Water (ENACW) mass of subtropical origin, whose archetypal concentrations of DO are initially low, would be ventilated by eddy-induced mixing with more oxygenated ENACW of subpolar origin (Pèrez et al., 2001).

Moreover, diatoms growth is thought to be positively correlated with the upwelling-driven nitrate inputs (Sarhou et al., 2005); in contrast, the growth of other planktonic groups can be insensitive to and even

limited by newly-upwelled nitrates (Mahaffey, 2005), especially when colimitation prevails or in the absence of necessary micro-nutrients.

The low-complexity O₂PZ model was directly implemented into the CROCO model following one of the already-embedded biogeochemical modules; it allows maintaining the full capabilities and versatility of this community code while gaining in computing efficiency (allowing extensive sensitivity studies and the consideration of submesoscale dynamics in oxygen cycling) as compared to the more complex biogeochemical modules already available within CROCO.

In the coupled model, the time evolution of DO, P and Z concentrations are given by, respectively:

$$\begin{aligned} \frac{\partial [O_2]}{\partial t} + u\frac{\partial [O_2]}{\partial x} + v\frac{\partial [O_2]}{\partial y} + w\frac{\partial [O_2]}{\partial z} = k_H (\frac{\partial^2 [O_2]}{\partial x^2} + \frac{\partial^2 [O_2]}{\partial y^2}) + \frac{\partial}{\partial z}(\langle [O_2] 'w' \rangle - \\ k_V \frac{\partial [O_2]}{\partial z}) + Va ([O_2] - [O_2]_{sat}) + AJ(z)f([O_2])[P] - u_r([O_2],[P]) - v_r([O_2],[Z]) - m[O_2], \end{aligned} \quad (1)$$

$$\begin{aligned} \frac{\partial [P]}{\partial t} + u\frac{\partial [P]}{\partial x} + v\frac{\partial [P]}{\partial y} + w\frac{\partial [P]}{\partial z} = k_H (\frac{\partial^2 [P]}{\partial x^2} + \frac{\partial^2 [P]}{\partial y^2}) + \frac{\partial}{\partial z}(\langle [P] 'w' \rangle - k_V \frac{\partial [P]}{\partial z}) + \\ l(N)g([O_2],[P]) - e([P],[Z]) - \sigma[P], \end{aligned} \quad (2)$$

$$\begin{aligned} \frac{\partial [Z]}{\partial t} + u\frac{\partial [Z]}{\partial x} + v\frac{\partial [Z]}{\partial y} + w\frac{\partial [Z]}{\partial z} = k_H (\frac{\partial^2 [Z]}{\partial x^2} + \frac{\partial^2 [Z]}{\partial y^2}) + \frac{\partial}{\partial z}(\langle [Z] 'w' \rangle - k_V \frac{\partial [Z]}{\partial z}) + \\ \kappa([O_2])e([P],[Z]) - \mu[Z], \end{aligned} \quad (3)$$

where (u, v, w) is the 3D velocity field, k_H and k_V are the horizontal and vertical tracer diffusivities, and $\langle \dots \rangle$ are the vertical turbulent fluxes. The biogeochemical model O₂PZ (SP2015) defines the source terms of DO, P and Z in the coupled model. It simulates seven biogeochemical reactions between the three compartments (Fig. 2) as follows: in the DO equation (Eq. 1),

On top of the oxygen that is produced and consumed within marine ecosystems, a considerable part of dissolved oxygen eventually becomes gaseous and is then exchanged at the ocean-atmosphere interface, contributing to the estimations that more than one half of atmospheric oxygen is produced in the ocean (Harris, 1986). The remaining term of Eq. (2) is the air-sea flux of O₂, which is the product of the gas transfer velocity Va , that depends on the square of the wind speed and on the Schmidt number (Wanninkhof, 1992), with the difference of the oceanic DO concentration and the solubility of O₂ in seawater.

This term is included here to circumvent the absence of nutrient limitation in the original O₂PZ model of SP2015. We chose to add a parametrization instead of a new equation for the nutrients because this last option would necessarily increase the complexity of the model.

The cross-shore wind component is zero in all cases. Despite the fact that “true” wind patterns observed over Western Iberia are undoubtedly more variable (both in terms of direction and magnitude) than our idealized forcing inspired from a specific campaign, it provides the quickest development of a clear upwelling front generating small-scale instabilities. Note that sensitivity tests were performed (not shown) and revealed that the model responses are qualitatively similar among different wind strengths, given that the magnitude is high enough to ensure the development of the unstable upwelling front.

We compared the full ranges of densities ρ , DO concentrations $[O_2]$, and chlorophyll-a concentrations $[Chl-a]$ of the reference simulation to all compiled measurements collected during the MOUTON campaign. Given the low-complexity of the biogeochemical model and the highly idealized physical setting, a fully quantitative comparison is out of scope, however we confirm that the coupled model reproduces qualitatively well the ρ - $[O_2]$ and ρ - $[Chl-a]$ relationships obtained from in-situ observations.

In a qualitative sense our idealized model results are similar to more realistic model studies such as Gutknecht *et al.* (2013) which in their modelling study of the Benguela upwelling region found a low $[O_2]$ plume for the climatological month of December at the shelf edge, and to observational studies such as Hales *et al.* (2006), which for the Oregon coast, measured $[O_2]$ of 70-110 mmol m⁻³ in upwelled water at the shelf break, about 200 mmol m⁻³ less than at the surface, which is the same range of the vertical gradient simulated here.

The low-complexity O₂PZ model accounts for oxygen production by photosynthesis and consumption by both respiration and remineralization but its simplicity does not allow to include other oceanographic

processes that could influence oxygen cycling over shallow shelves, such as for instance the complex benthic-pelagic coupled processes (Capet et al., 2016).

compare

qualitatively

In permanent Oxygen Minimum Zones (OMZs), changes in physical forcing (e.g. wind regime) and/or biological characteristics (e.g. size structure or functional types) can have dire implications for marine ecosystems and fisheries management. Indeed, the measured expansion of the Tropical Atlantic and Pacific OMZs (Stramma et al., 2008) implies a shallower upper boundary of the low O₂ core and an increased sensitivity of oxygen levels over the continental shelf to upwelling winds, which are indeed predicted to intensify with climate change (Sydeman et al., 2014). Future work could be focused on understanding this high sensitivity and on anticipating how it would affect the stability of the coupled-system in a changing climate.

This results in a

that

Álvarez-Salgado, X.A., Nieto-Cid, M., Álvarez, M., Pérez, F.F., Morin, P., Mercier, H.: New insights on the mineralization of dissolved organic matter in central, intermediate, and deep water masses of the northeast North Atlantic. *Limnol. Oceanogr.* 58, 681–696. doi.org/10.4319/lo.2013.58.2.0681, 2013.

Capet, A., Meysman, F.J.R., Akoumianaki, I., Soetaert, K., Grégoire, M.: Integrating sediment biogeochemistry into 3D oceanic models: A study of benthic-pelagic coupling in the Black Sea. *Ocean Modelling* 101, 83–100. doi.org/10.1016/j.ocemod.2016.03.006, 2016.

Castro, C.G., Nieto-Cid, M., Álvarez-Salgado, X.A., Pérez, F.F.: Local remineralization patterns in the mesopelagic zone of the Eastern North Atlantic, off the NW Iberian Peninsula. *Deep Sea Research Part I: Oceanographic Research Papers* 53, 1925–1940. doi.org/10.1016/j.dsr.2006.09.002, 2006.

Laffoley, D. and Baxter, J., 2019, *Ocean deoxygenation : everyone's problem : causes, impacts, consequences and solutions*, IUCN Report, Gland, Switzerland, 562 pages, doi.org/10.2305/IUCN.CH.2019.13.en

Pérez, F.F., Castro, C.G., Álvarez-Salgado, X.A., Ríos, A.F.: Coupling between the Iberian basin — scale circulation and the Portugal boundary current system: a chemical study. *Deep Sea Research Part I: Oceanographic Research Papers* 48, 1519–1533. doi.org/10.1016/S0967-0637(00)00101-1, 2001.

Sarthou, G., Timmermans, K.R., Blain, S., Tréguer, P.: Growth physiology and fate of diatoms in the ocean: a review. *Journal of Sea Research, Iron Resources and Oceanic Nutrients - Advancement of Global Environmental Simulations* 53, 25–42. doi.org/10.1016/j.seares.2004.01.007, 2005.

Stramma, L., Johnson, G.C., Sprintall, J., Mohrholz, V.: Expanding Oxygen-Minimum Zones in the Tropical Oceans. *Science* 320, 655–658. doi.org/10.1126/science.1153847, 2008.

Sydeman, W.J., García-Reyes, M., Schoeman, D.S., Rykaczewski, R.R., Thompson, S.A., Black, B.A., Bograd, S.J.: Climate change and wind intensification in coastal upwelling ecosystems. *Science* 345, 77–80. doi.org/10.1126/science.1251635, 2014.

Wanninkhof, R.: Relationship between wind speed and gas exchange over the ocean, *Journal of Geophysical Research*, 97(C5), 7373, doi:10.1029/92JC00188, 1992.

Effects of upwelling duration and phytoplankton growth regime on dissolved oxygen levels in an idealized Iberian Peninsula upwelling system

J. H. Bettencourt^{1*}, V. Rossi², L. Renault¹, P. Haynes³, Y. Morel¹, V. Garçon¹

¹LEGOS, University of Toulouse, CNES, CNRS, IRD, UPS, Toulouse 31400, France

²MIO (UM 110, UMR 7294), CNRS, Aix-Marseille Univ., Univ. Toulon, IRD, 13288, Marseille, France

³Department of Applied Mathematics and Theoretical Physics, University of Cambridge, England

*Correspondence to:

J. H. Bettencourt (joao.bettencourt@tecnico.ulisboa.pt)

Marine Environment Group

CENTEC - Centre for Marine Technology and Ocean Engineering

Instituto Superior Técnico (Pavilhão Central)

1049-001 Lisboa

Portugal

Abstract. We apply a coupled modelling system composed of a state-of-the-art hydrodynamical model and a low complexity biogeochemical model to an idealized Iberian Peninsula upwelling system to identify the main drivers of dissolved oxygen variability and to study its response to changes in the duration of the upwelling season and in phytoplankton growth regime. We find that the export of oxygenated waters by upwelling front turbulence is a major sink for nearshore dissolved oxygen. In our simulations of summer upwelling, when phytoplankton population is generally dominated by diatoms whose growth is largely enhanced by nutrient input, net primary production and air-sea exchange compensate dissolved oxygen depletion by offshore export over the shelf. A shorter upwelling duration causes relaxation of upwelling winds and a decrease in offshore export, resulting in a slight increase of net dissolved oxygen enrichment in the coastal region as compared to longer upwelling durations. When phytoplankton is dominated by groups less sensitive to nutrient inputs, growth rates decrease and the coastal region becomes net heterotrophic. Together with the physical sink, this lowers the net oxygenation rate of coastal waters, that remains positive only because of air-sea exchanges. These findings help disentangling the physical and biogeochemical controls of dissolved oxygen in upwelling systems and, together with projections of increased duration of upwelling seasons and phytoplankton community changes, suggest that the Iberian coastal upwelling region may become more vulnerable to hypoxia and deoxygenation.

1 Introduction

~~[Deleted Text] Marine hypoxia is an increasing global concern that is exacerbated by climate change, directly through warming-induced increase of stratification and decrease of oxygen solubility, and indirectly by changes in circulation and wind forcing (Levin, 2018).~~ Declining dissolved oxygen (DO) in the world ocean and coastal realm impacts all marine life, from microbes to higher trophic levels (Breitburg et al., 2018), with consequences ranging from ecological adaptations and shifts (Gilly et al., 2013), changes of biogeochemical activity (Wright et al., 2012) to mass mortality events (Diaz and Rosenberg, 2008) and biodiversity restructuring (Vaquer-Sunyer and Duarte, 2008).

Coastal waters are generally eutrophic and characterized by substantial planktonic productivity at the surface which favours oxygen consumption through remineralization of sinking organic matter, leading to low levels of DO in subsurface and near-bottom waters. Highly productive surface waters are typical of coastal upwelling regions and sustain socio-economically important ecosystems. ~~Upwelling systems are thus especially sensitive to deoxygenation (Paulmier and Ruiz-Pino, 2009) and to episodic hypoxia events with deleterious effects on marine life and human activities such as fisheries (Grantham et al., 2004;~~

~~Hales et al., 2006; McClatchie et al. 2010; Roegner et al., 2011).~~ [Inserted text] Upwelling systems are thus especially sensitive to episodic and long-term changes in DO levels with deleterious effects on marine life and human activities such as fisheries (Grantham et al., 2004; Hales et al., 2006; Paulmier and Ruiz-Pino, 2009; McClatchie et al. 2010; Roegner et al., 2011).

The western Iberian Peninsula Upwelling System (IPUS) is the northern branch of the Canary Upwelling System where the intra-annual variability of alongshore winds produce a seasonal upwelling/downwelling cycle (Wooster et al., 1976). In the summer and early fall, the Azores High migrates northward, causing a poleward alongshore wind that forces offshore Ekman transport of surface waters and upwelling of subsurface waters, while downwelling prevails the rest of the year. Long-term studies of the seasonal upwelling in the IPUS have pointed to a weakening of upwelling winds over multidecadal time scales (Sousa et al., 2017), but simulations of future climate indicate an enhancement of the upwelling due to poleward migration of the Azores High and a lengthening of the upwelling season (Miranda et al., 2013; Rykaczewski et al., 2015; Sousa et al., 2017).

During the upwelling season, hydrographic and biogeochemical variability is primarily determined by the wind forcing that controls the inflow of offshore deep water masses onto the shelf (Alvarez-Salgado *et al.*, 1993). ~~DO levels in these subsurface waters are thought to diminish during the upwelling season due to strong remineralization of sinking organic matter as well as to mixing with poorly-ventilated waters of subtropical origins (Castro et al., 2006). Overall, DO appears to partly control the remineralization of dissolved organic carbon in the IPUS and more generally in key water masses of the North Atlantic (Alvarez-Salgado et al. 2013).~~

DO, in addition of being transported by the Ekman upwelling circulation, is also affected by the turbulent component of the circulation, characterized by sub/mesoscale fronts, filaments and eddies (Bettencourt et al., 2015; Capet et al., 2008; Chaigneau et al., 2009; Marchesiello et al., 2003; Montes et al., 2014; Vergara et al., 2016). These structures have a strong influence on the cross-shore transport and on the vertical redistribution of biogeochemical tracers (Bettencourt et al., 2017; Combes et al., 2013; Gruber et al., 2011; Hernández-Carrasco et al., 2014; Nagai et al., 2015; Renault et al., 2016; Rossi et al., 2013). ~~In the Iberian basin, the Eastern North Atlantic Central Water (ENACW) mass of subtropical origin, whose archetypal concentrations of DO are initially low, would be ventilated by eddy-induced mixing with more oxygenated ENACW of subpolar origin (Pérez et al., 2001).~~

From the biological perspective, the planktonic community structure can also affect DO in the water column, as this results from the balance between oxygen production by photo-autotrophs and respiration by both auto and heterotrophs. Changes in the community composition should lead to changes in the DO budget of the continental shelf. In the Iberian upwelling, planktonic blooms tend to be dominated by large cells (micro-phytoplankton) such as diatoms (Moncoiffé et al., 2000; Rossi et al., 2013), that have lower respiration to photosynthesis ratios than dinoflagellates or cyanobacteria (López-Sandoval et al., 2014). ~~Moreover, diatoms growth is thought to be positively correlated with the upwelling-driven nitrate inputs; in contrast, the growth of other planktonic groups can be insensitive to and even limited by newly-upwelled nitrates, especially when colimitation prevails or in the absence of necessary micro-nutrients.~~ Moreover, diatoms growth is thought to be positively correlated with the upwelling-driven nitrate inputs (Sarhou et al., 2005); in contrast, the growth of other planktonic groups can be insensitive to and even limited by newly-upwelled nitrates (Mahaffey, 2005), especially when colimitation prevails or in the absence of necessary micro-nutrients. Thus, changes in the relative dominance of functional groups in the community can lead to different autotrophy/heterotrophy regimes and total DO levels.

In this paper, we perform a process-oriented study coupling an idealized IPUS configuration of a hydrodynamic model with a low-complexity biogeochemical model centred on oxygen. We focus on the mechanisms of DO change to assess the relative role/importance of physical (upwelling duration) and biogeochemical (functional planktonic community) processes in setting DO levels and distribution. Previous studies have focused on the seasonal and climatological modelling of the planktonic ecosystems and of dissolved oxygen (Marta-Almeida et al., 2012; Reboreda et al., 2014, 2015). Here, the spatio-temporal scales studied are shorter since we are interested in the variations and forcing mechanisms of DO levels in response to

successive and short-lived upwelling pulses, commonly observed in the IPUS during the upwelling season. The coupled physical-biogeochemical model is presented in Sect. 2; our results are shown and analysed in Sect. 3. We then discuss our findings and conclude in Sect. 4.

2 Materials and methods

2.1 The coupled model

The idealized IPUS consist in a meridionally-oriented stretch of continental shelf with constant bathymetry and limited zonally by the coast and the open ocean (Fig. 1). The domain has 300 km of length and width, with a shelf width of 50 km, which is characteristic of the Iberian shelf at 41° N. The resolution of the spatial grid is 500 m, allowing the simulation of summer upwelling seasons up to 90-day duration, with the associated upwelling front dynamics – meso and submesoscale vortices and filaments - within acceptable computing time limits.

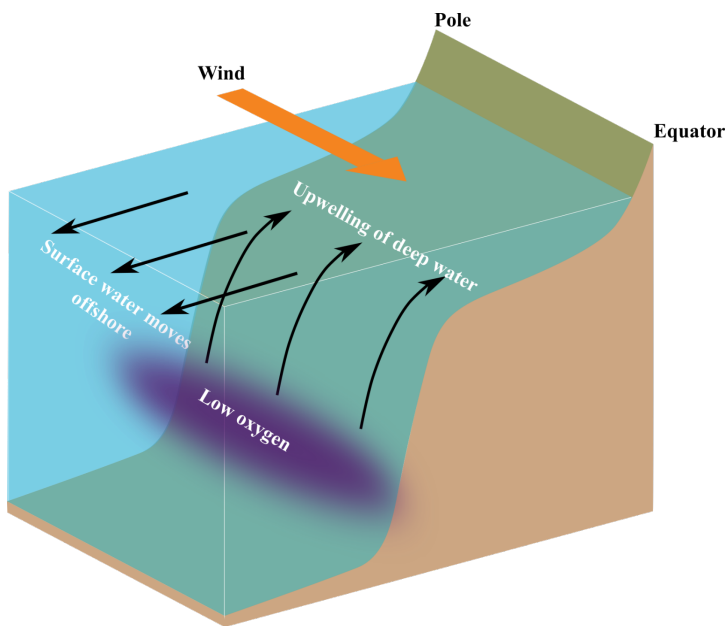


Figure 1. Idealized coastal upwelling configuration. The domain is periodic in the meridional (pole-equator) direction.

The physical-biogeochemical model couples the 3-dimensional Regional Ocean Modelling System ROMS (Shchepetkin, 2015; Shchepetkin and McWilliams, 2005), in its Coastal and Regional Ocean Community (CROCO) version (Debreu et al., 2012) to the low-complexity Oxygen-Phytoplankton-Zooplankton biogeochemical model of Petrovskii et al. (2017) and Sekerci and Petrovskii (2015), hereafter SP2015. Oxygen is used as the main model currency since it is central for the functioning of marine ecosystems (Breitburg et al., 1997, 2018). Oxygen is also at the heart of the photosynthesis and carbon fixation metabolic pathways for prokaryotic and eukaryotic algae, being a major electron acceptor (Mackey et al., 2008; Zehr and Kudela, 2009). and is needed for many biogeochemical reactions, including those involved in remineralization, that constantly occur in the oceanic water column. ~~On top of the oxygen that is produced and consumed within marine ecosystems, a considerable part of dissolved oxygen eventually become gaseous and is then exchanged at the ocean-atmosphere interface, contributing to the estimations that more than one half of atmospheric oxygen is produced in the ocean (Harris, 1986).~~ The low-complexity O₂PZ model was directly implemented into the CROCO model following one of the already-embedded biogeochemical modules; it allows maintaining the full capabilities and versatility of this community code while gaining in computing efficiency (allowing extensive sensitivity studies and the consideration of submesoscale dynamics in oxygen cycling) as compared to the more complex biogeochemical modules already available within CROCO.

ROMS–CROCO is a hydrostatic primitive equation model, formulated in finite differences with time-splitting in the barotropic (fast) mode and the baroclinic (slow) mode. It uses a terrain following vertical discretization in σ coordinates with 40 vertical levels. The prognostic variables are the horizontal barotropic and baroclinic momentum components, temperature and salinity. Free-surface displacement and vertical momentum are diagnostic variables. Horizontal advection of momentum and tracers is calculated from a 3rd order upstream biased scheme. Horizontal mixing is Laplacian, along iso- σ surfaces, with diffusivity coefficients of $2 \text{ m}^2\text{s}^{-1}$ and $0.2 \text{ m}^2\text{s}^{-1}$ for momentum and tracers respectively. Vertical mixing uses the KPP scheme of Large *et al.* (1994). The model is initialized from rest; the initial temperature and salinity distributions are uniform in the horizontal and the vertical profiles are taken from the World Ocean Atlas 2013 climatology (Boyer et al., 2013). Initial fields of the biogeochemical tracers (O_2 , P and Z) are also horizontally homogeneous and their vertical profiles are obtained from a water column (e.g. 1-dimensional) model version of the O_2PZ model (not shown). The channel is periodic in the meridional boundaries; the eastern boundary (coast) is modelled as a free-slip wall and the western one (open ocean) is open with radiative boundary conditions for momentum and tracers. Within the westernmost 50 km, a sponge layer is applied with increased horizontal viscosity of $200 \text{ m}^2\text{s}^{-1}$ and a nudging time-scale of 3 days in order to nudge all prognostic variables to their initial values over the offshore region. The bottom stress formulation is logarithmic with a roughness height of 0.01 m. The model is forced by a cyclic uniform wind field. To promote the destabilization of the upwelling front, we introduce a small spatial perturbation to the wind field, whose amplitude is less than 1% of the total wind speed and with characteristic wavelengths of 10 km and 50 km in the alongshore and cross-shore directions, respectively.

~~In the coupled model, the time evolution of a tracer concentration C is given by:~~

~~$$\partial C/\partial t + u\partial C/\partial x + v\partial C/\partial y + w\partial C/\partial z = k(\partial^2 C/\partial x^2 + \partial^2 C/\partial y^2 + \partial^2 C/\partial z^2) + F_A + Q_C \quad (1)$$~~

~~where (u, v, w) is the 3D velocity field, k the tracer diffusivity, F_A is the air-sea oxygen exchange flux term (positive when the ocean receives oxygen) and Q_C is the source/sink term for the tracer C , here defined by the biogeochemical model O_2PZ (SP2015). It simulates seven biogeochemical reactions between the three compartments (Fig. 2) as follows:~~

~~$$Q_{\text{O}_2} = AJ(z)f([\text{O}_2])[P] - u_r([\text{O}_2], [P]) - v_r([\text{O}_2], [Z]) - m[\text{O}_2] \quad (2)$$~~

~~$$Q_P = l(N)g([\text{O}_2], [P]) - e([P], [Z]) - \sigma[P] \quad (3)$$~~

~~$$Q_Z = \kappa([\text{O}_2])e([P], [Z]) - \mu[Z] \quad (4)$$~~

~~In the source/sink term expression for DO (Eq. 2),~~

In the coupled model, the time evolution of DO, P and Z concentrations are given by, respectively:

$$\partial[\text{O}_2]/\partial t + u\partial[\text{O}_2]/\partial x + v\partial[\text{O}_2]/\partial y + w\partial[\text{O}_2]/\partial z = k_H(\partial^2[\text{O}_2]/\partial x^2 + \partial^2[\text{O}_2]/\partial y^2) + \partial/\partial z(\langle[\text{O}_2]'w'\rangle - k_V\partial[\text{O}_2]/\partial z) + Va([\text{O}_2] - [\text{O}_2]_{\text{sat}}) + AJ(z)f([\text{O}_2])[P] - u_r([\text{O}_2], [P]) - v_r([\text{O}_2], [Z]) - m[\text{O}_2], \quad (1)$$

$$\partial[P]/\partial t + u\partial[P]/\partial x + v\partial[P]/\partial y + w\partial[P]/\partial z = k_H(\partial^2[P]/\partial x^2 + \partial^2[P]/\partial y^2) + \partial/\partial z(\langle[P]'w'\rangle - k_V\partial[P]/\partial z) + l(N)g([\text{O}_2], [P]) - e([P], [Z]) - \sigma[P], \quad (2)$$

$$\partial[Z]/\partial t + u\partial[Z]/\partial x + v\partial[Z]/\partial y + w\partial[Z]/\partial z = k_H(\partial^2[Z]/\partial x^2 + \partial^2[Z]/\partial y^2) + \partial/\partial z(\langle[Z]'w'\rangle - k_V\partial[Z]/\partial z) + \kappa([\text{O}_2])e([P], [Z]) - \mu[Z], \quad (3)$$

where (u, v, w) is the 3D velocity field, k_H and k_V are the horizontal and vertical tracer diffusivities, and $\langle \dots \rangle$ are the vertical turbulent fluxes. The biogeochemical model O_2PZ (SP2015) defines the source terms of DO, P and Z in the coupled model. It simulates seven biogeochemical reactions between the three compartments (Fig. 2) as follows: in the DO equation (Eq. 1), the term $AJ(z)f([\text{O}_2])$ is the rate of O_2 production by photosynthesis and is modelled by a Monod parametrization $f([\text{O}_2]) = c_0/([\text{O}_2] + c_0)$, where c_0 is a half-saturation constant. The term $J(z) = 1 - \exp(-\alpha PAR(z)/A)$ represents the light dependency of photosynthesis, with $\alpha = 30$ and the photosynthetically available radiation $PAR(z) = PAR(0) \exp(-k_w z)$, with $PAR(0) = 355.19 \text{ W/m}^2$ and $k_w = 0.04 \text{ m}^{-1}$.

We distinguish here the terms ‘photosynthesis’ from ‘carbon fixation’ (Behrenfeld et al., 2008). Indeed, ‘photosynthesis’ is the production of ATP and NADPH by the photosynthetic electron transport (PET) chain and these two products are referred

to as ‘photosynthate’. By contrast, ‘carbon fixation’ refers to the use of photosynthate by the Calvin cycle to produce simple organic carbon products independently of light. SP2015 chose to highlight these two stages in their model formulation by decoupling carbon fixation from photosynthesis. The respiration by phytoplankton u_r is given by $u_r([O_2],[P])=\delta[O_2][P]/([O_2]+c_2)$, where δ is the maximum per capita phytoplankton respiration rate and c_2 is the half saturation constant. Zooplankton respiration is similar: $v_r([O_2],[Z])=v[O_2][Z]/([O_2]+c_3)$ and the constants v and c_3 have the same functions as in u_r . A Monod function is a logical formulation to have respiration depending on oxygen concentration since if the fluid environment becomes anoxic, then plankton cannot breathe so that respiration terms u_r and v_r vanish. . The fourth term parametrizes bacterial respiration (oxygen loss due to natural depletion, e.g. remineralization). **On top of the oxygen that is produced and consumed within marine ecosystems, a considerable part of dissolved oxygen eventually becomes gaseous and is then exchanged at the ocean-atmosphere interface, contributing to the estimations that more than one half of atmospheric oxygen is produced in the ocean (Harris, 1986).The remaining term of Eq. (2) is the air-sea flux of O_2 , which is the product of the gas transfer velocity velocity Va , that depends on the square of the wind speed and on the Schmidt number (Wanninkhof, 1992), with the difference of the oceanic DO concentration and the solubility of O_2 in seawater.**

In Eq. (32), phytoplankton growth $g([O_2],[P])$ is given by a linear growth term $\alpha([O_2])[P]$ minus intraspecific competition $\gamma [P]^2$, where γ is the intraspecific competition intensity. The per capita growth rate is a Monod function $\alpha([O_2])=B[O_2]/([O_2]+c_1)$ where B is the maximum per capita growth rate in the large $[O_2]$ limit and c_1 is the half saturation constant. The $l(N)$ term is a Monod function $l(N)=k_1N(\rho)/(k_2 + N(\rho))$, where $N(\rho)$ is a parametrization of nutrient availability based on the nitrate-density (ρ) relationships measured during an oceanographic cruise which surveyed the IPUS during upwelling season (the 2007 MOUTON campaign, see also Rossi et al. 2010; 2013). **This term is included here to circumvent the absence of nutrient limitation in the original O_2PZ model of SP2015. We chose to add a parametrization instead of a new equation for the nutrients because this last option would necessarily increase the complexity of the model.**

SP2015 used a formulation where high oxygen increases phytoplankton growth but limits oxygen production by photosynthesis. The Warburg effect (Turner, 1962) corresponds to the decrease of the photosynthesis rate at high oxygen concentrations so the choice of $f([O_2])$ where high $[O_2]$ limits $[O_2]$ production makes sense. Moreover oxygen stimulates photorespiration which reduces photosynthesis yield. As soon as a water molecule (H_2O) undergoes photolysis in the chloroplast of oxygenic photosynthetic organisms, O_2 as well as ATP (Adenosine TriPhosphate) are being produced through both photosystems I and II. The products of photosynthesis (ATP) then enters the Calvin cycle to convert carbon dioxide and other compounds into glucose, that is the food that autotrophs need to grow. As such, we can relate the growth term $\alpha([O_2])$ to $[O_2]$ with a Monod function so as high $[O_2]$ corresponds to high growth rate. The predation term is $e([P],[Z])=\beta[P][Z]/([P]+h)$ where β is the maximum predation rate and h is the half saturation constant. Phytoplankton mortality is $\sigma[P]$. Regarding zooplankton, its feeding efficiency is a function of oxygen concentration $\kappa([O_2])=\eta[O_2]^2/([O_2]^2+c_4^2)$ where η is the maximum feeding efficiency and c_4 is the half-saturation constant. Zooplankton mortality is given by $\mu[Z]$.

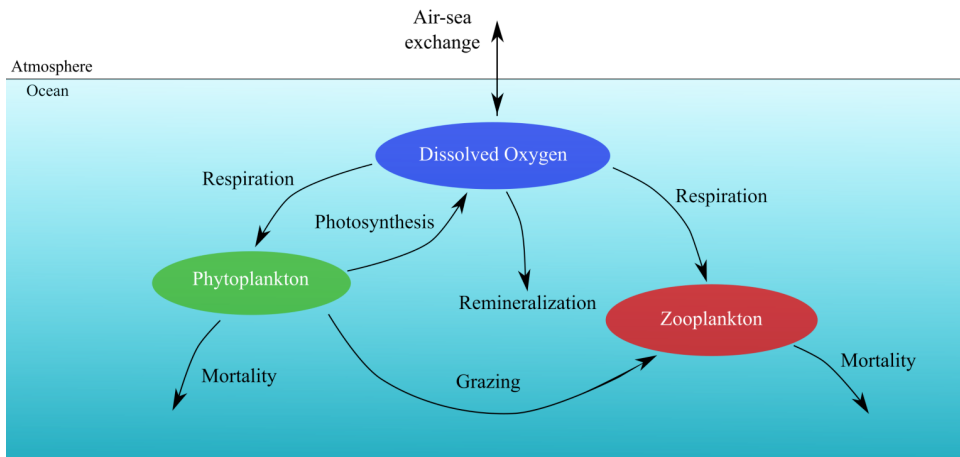


Figure 2. The Oxygen-Phytoplankton-Zooplankton model of SP2015, adapted to the oceanic environment.

The parameters of the O₂PZ model were adjusted so that its 0-D version (without advection or diffusion, see table A3) has a steady state at values representative of the IPUS (see Appendix A).

2.2 Simulations

The coupled model is initialized at rest. Biogeochemical tracers are initialized from vertical profiles (Fig. 3(a)) obtained by a water column 1D model of the O₂PZ model that was run for long enough time to reach stable vertical distributions (not shown). Using these profiles instead of climatological initial conditions allows reducing the 3D coupled model drift (not shown). Initial temperature and salinity profiles (Fig. 3(b)) were taken from the World Ocean Atlas 2013 (WOA13, Boyer et al., 2013) data at 12°W and 41°N.

Our set of simulations (Table 1) is designed to investigate the sensitivity of the coastal DO inventory to upwelling duration and community structure (diatom dominated or not). We choose the duration of upwelling-favourable wind instead of its magnitude as a control factor because it has been shown to be a better predictor of coastal hypoxia (Feng et al., 2012; Forrest et al., 2011; Zhang et al., 2018). Community structure is set through the growth regime of the primary producers (phytoplankton) with respect to nutrient input. Thus, a diatom dominated regime is simulated using enhanced growth rates due to nutrient input – the *(E)nhanced* runs - while a non-diatom dominated regime is simulated with growth rates *(N)eutral* to and *(L)imited* by nutrient input. We test the sensitivity of our coupled system to the relative dominance of diatoms in the community as they have been suggested to decline over the long-term, being gradually replaced by dinoflagellates and cyanobacteria (Gregg et al., 2017).

The effects of upwelling season length are studied by running two simulations where the number of upwelling favourable wind cycles are 4 and 9, maintaining a total simulation time of 90 days and considering a diatom dominated phytoplankton community. The wind profiles (Fig. 3(c)) are based on the cyclic wind pulses that are characteristic of the summer / early fall upwelling favourable conditions in the IPUS: 10-day pulses with maximum wind speed of 12 ms⁻¹ (Rossi et al., 2013; Torres et al., 2003). The cross-shore wind component is zero in all cases. Despite the fact that “true” wind patterns observed over Western Iberia are undoubtedly more variable (both in terms of direction and magnitude) than our idealized forcing inspired from a specific campaign, it provides the quickest development of a clear upwelling front generating small-scale instabilities. Note that sensitivity tests were performed (not shown) and revealed that the model responses are qualitatively similar among different wind strengths, given that the magnitude is high enough to ensure the development of the unstable upwelling front.

Table 1 Simulations. ECC is the reference simulation. All simulations are run for 90 days.

Simulation	P Growth (k_1, k_2)	Upwelling season
NCC	Neutral (1,0)	9 cycles
LCC	Limited (1,0.5)	9 cycles
ECC	Enhanced (2,0.5)	9 cycles
ECS	Enhanced (2,0.5)	4 cycles

In-situ observations of the IPUS, collected during the MOUTON 2007 campaign (Rossi et al., 2010; 2013), and compiled within the WOA13 (Boyer et al., 2013) are used not only to initialize but also to validate the outputs of our simulations. The ECC simulation used the wind forcing and phytoplankton growth regimes that most resemble the IPUS region and therefore was chosen as the reference simulation. ~~We compared the full ranges of densities ρ , DO concentrations [O₂], and chlorophyll-a concentrations [Chl-a] of the reference simulation to all compiled measurements collected during the MOUTON campaign. We confirm that the coupled model, although of low complexity, reproduces relatively well the ρ -[O₂] and ρ -[Chl-a] relationships obtained from in-situ observations, despite a slight underestimation of [O₂] and [Chl-a] (Fig. 4). Note however that the cruise was specially designed to sample high coastal chlorophyll concentrations observed from satellite, so the dataset used in the comparison is biased towards high chlorophyll conditions.~~

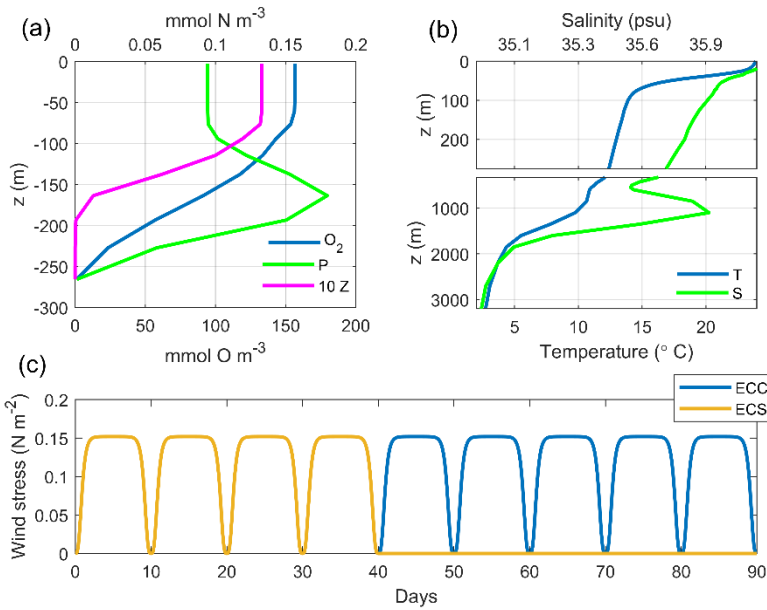


Figure 3. Initial conditions and wind forcing. (a) Initial profiles of O₂, P and Z. (b) Initial profiles of temperature (T) and salinity (S). (c) Wind forcing regimes; ECC: 9 wind cycles; ECS: 4 wind cycles.

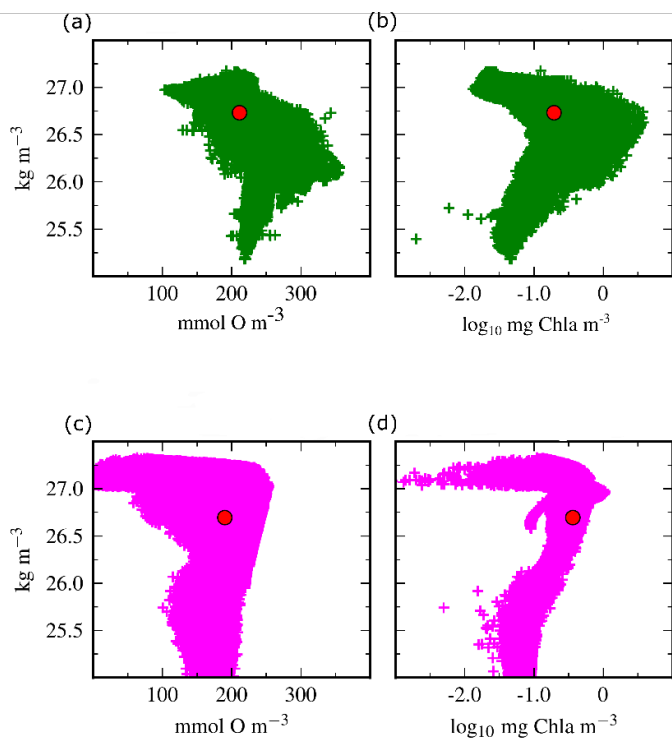


Figure 4. Validation of ECC simulation. a) Measured density vs. $[\text{O}_2]$; b) Measured density vs. $[\text{Chl-a}]$ (fluorescence as a proxy for Chl-a); c) Modeled density vs. $[\text{O}_2]$; d) Modeled density vs. $[\text{Chl-a}]$.

We compared the full ranges of densities ρ , DO concentrations $[\text{O}_2]$, and chlorophyll- a concentrations $[\text{Chl-a}]$ of the reference simulation to all compiled measurements collected during the MOUTON campaign. Given the low-complexity of the biogeochemical model and the highly idealized physical setting, a fully quantitative comparison is out of scope, however we confirm that the coupled model reproduces qualitatively well the ρ - $[\text{O}_2]$ and ρ - $[\text{Chl-a}]$ relationships obtained from in-situ observations.

3. Results and discussion

3.1 Dissolved Oxygen in the Idealized IPUS

Our coupled model reproduces well the upwelling circulation and the typical biological responses. Indeed, the upwelling of nutrient-rich waters induced by the mean wind-driven circulation promotes the growth of phytoplankton, leading to increased oxygen production by photosynthesis and the subsequent enrichment of oxygen in shelf waters ($x < 80$ km, Fig. 5(a)), as compared with the lower $[\text{O}_2]$ found in offshore waters ($x > 80$ km). It also shows a low $[\text{O}_2]$ cell ($\sim 50 \text{ mmol m}^{-3}$), at the subsurface over the outer-shelf (centred at 40 km and 60 m depth) because of the upwelling of low O_2 waters, consistent with the shelf low $[\text{O}_2]$ cell ($< 200 \mu\text{mol kg}^{-1}$) measured during the MOUTON cruise (e.g. Rossi et al. 2013). ~~Similarly, Gutknecht et al. (2013) in their modelling study of the Benguela upwelling region found a low $[\text{O}_2]$ plume for the climatological month of December at the shelf edge. For the Oregon coast, Hales et al. (2006) measured $[\text{O}_2]$ of 70-110 mmol m^{-3} in upwelled water at the shelf break, about 200 mmol m^{-3} less than at the surface, which is the same range of the vertical gradient simulated here.~~ In a qualitative sense our idealized model results are similar to more realistic model studies such as , Gutknecht et al. (2013) which in their modelling study of the Benguela upwelling region found a low $[\text{O}_2]$ plume for the climatological month of December at the shelf edge, and to observational studies such as Hales et al. (2006), which for the Oregon coast, measured $[\text{O}_2]$ of 70-110 mmol m^{-3} in upwelled water at the shelf break, about 200 mmol m^{-3} less than at the surface, which is the same range of the vertical gradient simulated here.

The dynamics of the ECC simulation (Appendix B), are consistent with those documented by Durski and Allen (2005). A mean Ekman upwelling transport is established, moving subsurface waters upwards near the coast. The eddy induced circulation (Cerovečki et al., 2009; Plumb and Ferrari, 2005) has the opposite sense to the mean circulation and is the strongest in the 50 to 100 km offshore range (Fig. B1). The result of the eddy induced onshore and downward circulation is mainly seen in the subduction of the oxygen rich waters just offshore of the shelf edge, as suggested by the spatial pattern of the eddy-stream-function (Fig. B1).

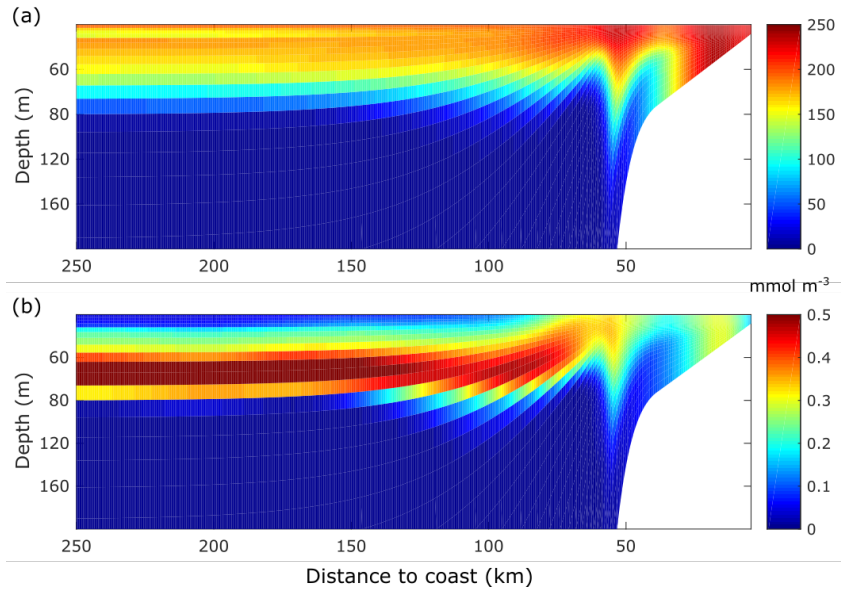


Figure 5. Mean [O₂], [P] fields of the ECC simulation. a) Time mean of along-shore averaged [O₂] field. b) Time mean of along-shore averaged [P] field. Time means are computed from day 20 to day 90.

The spatial coincidence between the high [O₂] and high phytoplankton concentration [P] near the coast (Fig. 5) reflects O₂ enrichment caused by photosynthetic production (see Sect. 3.2 for a budget analysis). Since oxygen limits phytoplankton growth in our model, the low [O₂] cell in the coast causes a matching low [P] cell at the same location. Further offshore, subsurface [P] and [O₂] decrease as phytoplankton growth is limited by the lack of nutrients in the euphotic zone.

The subsurface [P] maximum between 60 and 80 meters depth results from the trade-off between sufficient oxygen, light levels and nutrients availability. Consequently, the enhanced phytoplankton growth rate due to nutrients appears to compensate for the low oxygen levels, thus promoting phytoplankton growth. Moreover, the low [O₂] will maintain the zooplankton stocks at low levels, thus constraining the grazing pressure of zooplankton on phytoplankton.

The dominant length-scales, i.e. the inverse of the wave number where the alongshore [O₂] anomaly field spectrum has a maximum, vary with time and distance to coast (Fig. 6(a)). After day 30, between 50 and 150 km offshore we observe the emergence of dominant length scales of 150 km in an intermittent fashion, in a process that agrees with previous studies of the growth and decay of large mesoscale structures in coastal upwelling systems (Durski and Allen, 2005).

Slopes of time averaged spectra of alongshore [O₂] anomalies at three offshore locations (Fig. 6(b)) show, however, that submesoscale has also a marked effect on the [O₂] field. All spectra are shallower than the k^{-3} slope of geostrophic turbulence (Charney, 1971), implying that the submesoscale is prominent in our simulations (Capet et al., 2008). The spectrum at $x=50$ km is the shallowest and the closest to the $k^{-5/3}$ slope in the range $8.10^{-4} < k < 10^{-4}$. In the lower k range ($k < 10^{-5}$), the spectra at 50 and 100 km have higher energy than the spectrum at 200 km, as the dominant length-scale plot shows the largest dominant length-scales in the 50-150 km cross-shore region.

The Probability Density Function (PDF) of the [O₂] gradient norm (Fig. 6(c)) has a heavy tail distribution, associated with intermittency (Capet et al., 2008; Castaing et al., 1990). The existence of long tails in all PDF's indicates that sharp [O₂] gradients are ubiquitous in the channel.

Turbulence redistributes oxygen through fronts and filaments (strain-dominated regions) as well as vortices (rotation-dominated regions). To analyse this process, we use the Okubo-Weiss criterion γ , which separates turbulent velocity fields in strain-dominated ($\gamma > 0$) and rotation-dominated ($\gamma < 0$) regions. More specifically, we compute the daily average surface $[O_2]$ for each γ and binned shore distance x .

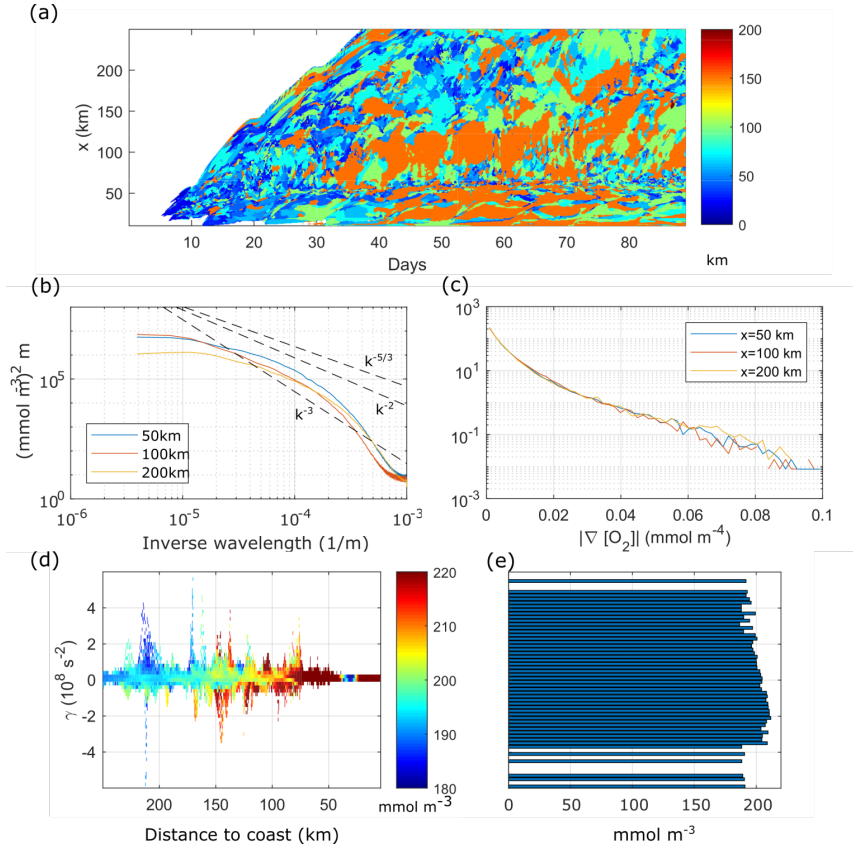


Figure 6. a) Peak wavelength of surface $[O_2]$ alongshore wavenumber spectrum as a function of time and offshore shore distance. b) Time mean surface $[O_2]$ alongshore wavenumber spectrum at $x=50$ km, 100 km, and 200 km offshore. $[O_2]$ spectra computed from anomalies with respect to alongshore mean. c) PDF of time mean surface $[O_2]$ gradient norm at $x=50$ km, 100 km, and 200 km. d) Instantaneous distribution of surface $[O_2]$ by x and γ at day 65. e) Distribution of x -averaged $[O_2]$ by γ at day 65. Time mean taken from day 20 to day 90.

For day 65, the $[O_2]$ distribution by (γ, x) (Fig. 6(d)) reproduces the cross-shore $[O_2]$ gradient of coastal elevated $[O_2]$ and lower offshore $[O_2]$ (the background gradient, see also Fig. 5 (a)), in the range $\gamma \sim 0$. Deviations from this background gradient are found along the cross-shore direction, as we move to larger $|\gamma|$, implying that $[O_2]$ anomalies with respect to the mean surface field are mainly found in filaments and vortices. Since the highest $[O_2]$ levels are found in the shelf region, due to photosynthetic production, their presence further offshore strongly suggests offshore export by turbulent structures. We emphasize that offshore transport of $[O_2]$ rich water results in a net loss of O_2 for the continental shelf region.

The $[O_2]$ anomalies found offshore in positive and negative γ regions highlight the transport and dispersion of O_2 by sub/mesoscale structures from the shelf to the open ocean. We find that although the mean $[O_2]$ as a function of γ (averaged over x in each γ bin) remains at ~ 200 mmol m^{-3} (Fig. 6 (e)), the $[O_2]$ distribution is biased toward negative γ , as found by Combes *et al.* (2013) for tracers in the California current. Our results are also in line with those of Lovecchio *et al.* (2017) that demonstrate the importance of mesoscale processes for the zonal advection of tracers, with a key role of eddies, especially offshore the upwelling front.

The relative importance of the physical versus the biological processes in controlling coastal oxygen dynamics was analysed in terms of the volume averaged rate of change of DO due to physics (advection and mixing), biology (photosynthesis,

community respiration and remineralization) and air-sea fluxes within a shelf control volume (from the coast to 50 km offshore and from the surface to 140 m depth) and averaged from day 20 to 90. The net enrichment rate, accounting for the physical and biological forcing, is positive ($2.26 \text{ mmol m}^{-3} \text{ d}^{-1}$) and so, over time, the coastal oxygen inventory increases. DO concentrations are increased by biogeochemical processes at a rate of $4.27 \text{ mmol m}^{-3} \text{ d}^{-1}$ and by air-sea exchange ($3.41 \text{ mmol m}^{-3} \text{ d}^{-1}$) but are limited by physical processes that remove O_2 from the coastal region ($-5.42 \text{ mmol m}^{-3} \text{ d}^{-1}$) through lateral advection.

3.2 Sensitivity of dissolved oxygen to upwelling duration and phytoplankton growth regimes

The reference simulation (ECC) has shown three major features: the appearance of sub-surface low $[\text{O}_2]$ cells because of the upwelling of O_2 poor waters, the O_2 enrichment of surface levels, and the appearance of an $[\text{O}_2]$ gradient between the biologically-mediated enrichment at the inner shelf and the depleted offshore region. This gradient is, on one hand maintained by the upwelling circulation and, on the other hand, smoothed out by the cross-shore transport of O_2 by small-scale vortices and filaments. These effects are driven by the wind regime, that controls the upwelling dynamics and instabilities, and by phytoplankton growth rate, which in turn affects phytoplankton concentrations. We now look at the sensitivity of the coupled model to these two drivers.

The continuous development of filaments and vortices in the ECC run maintains the offshore transport of dissolved oxygen (Fig. 7 (a)). The wind shutdown in the ECS run causes a gradual decrease of turbulence which implies a diminution of the $[\text{O}_2]$ redistribution by the cross-shore export physical processes, resulting in the creation of a sharper boundary between the oxygen-rich coastal waters and the depleted open ocean (offshore the upwelling front, Fig. 7 (b)).

The phytoplankton growth regime impacts the mean $[\text{O}_2]$ distribution since nutrient neutrality (NCC) or limitation (LCC) results in the decrease of $[\text{O}_2]$, when compared with the ECC run. The largest difference between the NCC and the ECC simulations (Fig. 8(a)), are observed in the coastal region, with maximum deviations from the ECC run up to 100 mmol m^{-3} . Offshore of the front, on the other hand, we find an increase of $[\text{O}_2]$ with respect to the ECC run, with the difference reaching $\sim 50 \text{ mmol m}^{-3}$ at $x=250 \text{ km}$. This positive difference is due to the absence of nutrient limitation, so that phytoplankton growth and oxygen production persist in the nutrient depleted surface levels.

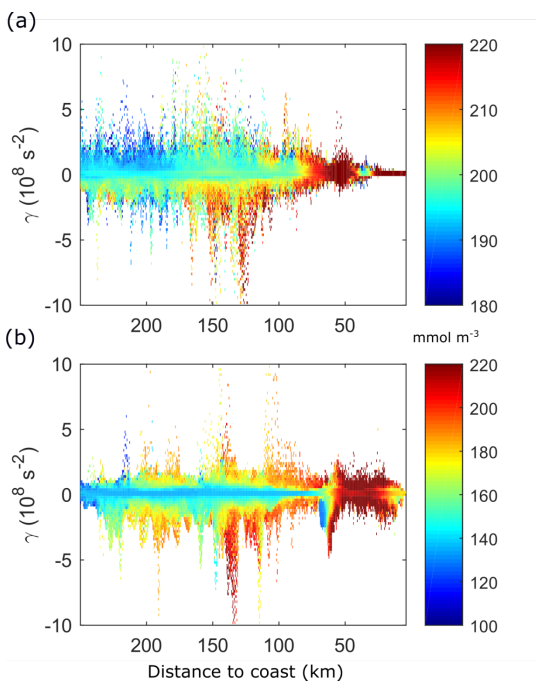


Figure 7. Time mean distribution of $[\text{O}_2]$ by x and γ . (a) ECC. (b) ECS. Time mean taken from day 20 to 90.

The difference between the LCC and ECC cases (Fig. 8(b)) is also the highest in the shelf region, slightly above 100 mmol m^{-3} . Offshore of the front ($x > 50 \text{ km}$), the difference reduces to less than 50 mmol m^{-3} , above 80 m depth, vanishing below this depth. In both cases, there is a signature of the low $[\text{O}_2]$ upwelling over the slope and shelf edge and the eddy-induced subduction just offshore of the front ($x = 50 \text{ km}$).

When analysing O_2 budgets in the coastal control volume, from shore to 50 km offshore and from surface to 200 m of depth, the short upwelling duration simulation (ECS) results in a slight increase of the shelf $[\text{O}_2]$ temporal mean net rate of change by 6% with respect to the ECC simulation (2.26 to $2.40 \text{ mmol m}^{-3} \text{ d}^{-1}$, Figure 9(a)). Although for ECS every term in the oxygen mean budget is smaller than for ECC, the physical sink decrease is slightly higher than the combined decrease in biological source and sink (Q_{O_2}) and air-sea exchange.

The changes in physical sink also occur faster than those in the biological terms. The wind cessation at day 40 causes an immediate decrease in the physical term (Fig. 9(b), lower panel) while only after day 70 can we observe a significant difference between the biological source/sink terms of both ECC and ECS simulations.

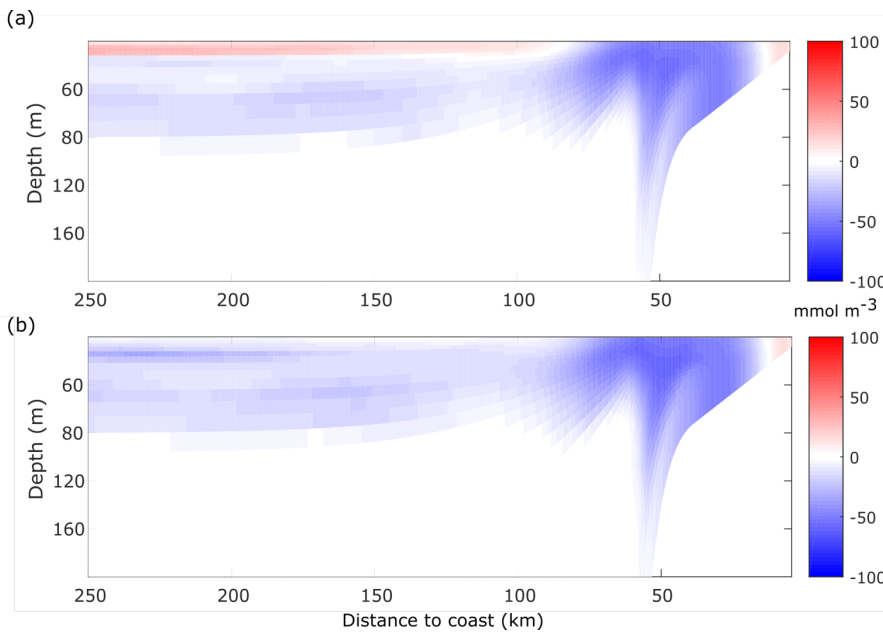


Figure 8. Difference in time mean dissolved oxygen with respect to the ECC run. (a) NCC. (b) LCC. Time mean taken from day 20 to 90

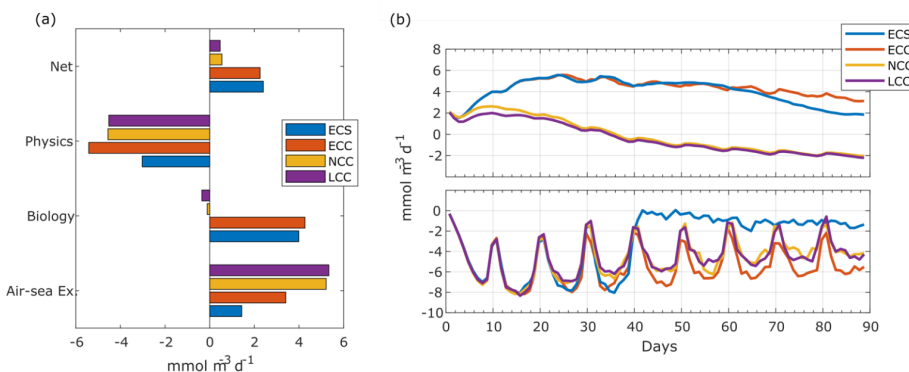


Figure 9. Dissolved Oxygen budgets in the coastal control volume. (a) Time mean rate of change of dissolved oxygen. Net value is the sum of Physical, Biological and Air-sea exchange source/sink terms. Physical terms are the sum of cross-shore, alongshore and vertical advectons as well as horizontal and vertical mixing. Biological term is oxygen photosynthetic production minus community respiration. Time mean taken from day 20 to 90. (b) Time series of average rate of change of dissolved oxygen in the coastal control volume due to biology (top) and physics (bottom).

Changes in the phytoplankton growth regime modify the physical-biological balance of oxygen in the coastal control volume. The coastal region is net autotrophic ($Q_{O_2} > 0$) for ECC ($Q_{O_2} = 4.27 \text{ mmol m}^{-3} \text{ d}^{-1}$) and ECS ($Q_{O_2} = 3.99 \text{ mmol m}^{-3} \text{ d}^{-1}$) but becomes slightly net heterotrophic ($Q_{O_2} < 0$) when the phytoplankton growth becomes neutral to (NCC, $Q_{O_2} = -0.11 \text{ mmol m}^{-3} \text{ d}^{-1}$) or limited by (LCC, $Q_{O_2} = -0.35 \text{ mmol m}^{-3} \text{ d}^{-1}$) nutrients (Fig. 9(a)). This modifies the $[O_2]$ gradients and the $[O_2]$ lateral advective fluxes and, as a result, the rate of oxygen loss through lateral advection decreases by about 15% for NCC and LCC, with respect to ECC. The air-sea exchange of O_2 is also affected by the growth regime changes, as lower $[O_2]$ will result in increased fluxes.

Overall, the phytoplankton growth regime has a stronger impact than the wind regime in the DO inventory in the shelf control volume. The NCC and LCC cases result in net rates of change of dissolved oxygen that are 75%-80% lower than in the reference case.

4 General discussion and conclusions

We built a coupled physical-biogeochemical model of an idealized seasonal coastal upwelling to study the effect of the upwelling season length and phytoplankton community structure on dissolved oxygen inventory. [The low-complexity \$O_2\$ PZ model accounts for oxygen production by photosynthesis and consumption by both respiration and remineralization but its simplicity does not allow to include other oceanographic processes that could influence oxygen cycling over shallow shelves, such as for instance the complex benthic-pelagic coupled processes \(Capet et al., 2016\).](#) While we used data from the Iberian Peninsula upwelling to initialize and [validate compare](#) the range of values simulated by our model, our idealized configuration allows to draw general conclusions about the mechanisms governing the dissolved oxygen levels over the continental shelf. When compared to measurements, our model reproduces [qualitatively well](#) the O_2 -density relationship as well as upwelling of oxygen-poor waters onto the shelf and the offshore transport of oxygen due to filaments and vortices. While the addition of air-sea exchange processes as well as our novel nutrient/density parametrization have probably contributed largely to simulate such realistic outputs despite the simple biogeochemical formulation, the coupled system could be further improved. One probably important task, that we keep for future studies, is to include realist subsurface O_2 inputs from oceanic currents, as it has been shown to control largely O_2 dynamics over the shelf [\(Montes et al., 2014; Reboreda et al., 2015\)](#).

Although there is a clear separation of coastal waters with high $[O_2]$ and offshore waters with low $[O_2]$, the turbulent lateral transport of high $[O_2]$ water disrupts this picture, as oxygen-rich upwelling filaments and vortices generated at the front and then travel offshore. This creates a sink of dissolved oxygen on the shelf that must be compensated by photosynthetic production and air-sea fluxes. In our reference simulation, with repeated upwelling wind cycle, the net $[O_2]$ rate of change was positive, owing to the predominance of the photosynthetic oxygen production and air-sea fluxes over the lateral transport of oxygen, that acts to remove it from the shelf region. When considering a shorter upwelling season (the ECS case with four 10-day upwelling wind cycles followed by wind cessation) reinforces somewhat the oxygen enrichment trend. When phytoplankton community is dominated by groups that show nutrient limitation or neutral growth (LCC and NCC cases), the biological source weakens and the shelf becomes net heterotrophic. The physical sink is also affected, producing a weaker loss of dissolved oxygen in the coastal upwelling. Air-sea exchange then maintains the (much lower) net oxygen enrichment trend. Our findings that the oxygen inventory net rate of change is inversely proportional to the duration of upwelling season is consistent with other studies (Adams et al., 2013; Siedlecki et al., 2015; Zhang et al., 2018) and, as the upwelling season duration in the IPUS is thought to increase in the future (Miranda et al., 2013; Wang et al., 2015), it suggests increased vulnerability of coastal regions to hypoxia and long-term deoxygenation. The result of lower phytoplankton growth rates driving the shelf region from autotrophy to heterotrophy also points to an increased risk of loss of dissolved oxygen if trends for community shifts towards smaller or less efficient phytoplankton (Gomes et al., 2014; Gregg et al., 2017; Head and Pepin, 2010; Zhai et al., 2013) are specifically confirmed for the IPUS. [In permanent Oxygen Minimum Zones \(OMZs\), changes in](#)

physical forcing (e.g. wind regime) and/or biological characteristics (e.g. size structure or functional types) can have dire implications for marine ecosystems and fisheries management. Indeed, the measured expansion of the Tropical Atlantic and Pacific OMZs (Stramma et al., 2008) implies a shallower upper boundary of the low O₂ core and an increased sensitivity of oxygen levels over the continental shelf to upwelling winds, which are indeed predicted to intensify with climate change (Sydeman et al., 2014). Future work could be focused on understanding this high sensitivity and on anticipating how it would affect the stability of the coupled-system in a changing climate.

Data availability

Simulated data are available upon request.

Appendix A. Determination of O₂PZ model parameters.

The biogeochemical component of the 3D coupled model (Eqs. (1), (2)-(4)) is a system of ODE's that computes the local time evolution of [O₂], [P] and [Z]. The ODE system accounts for the processes that move O₂, P and Z between different reservoirs. Each ODE of the model then expresses the input and output of the species from the specific reservoir. The dynamical properties the ODE's will therefore influence the global behaviour of the coupled physical-biogeochemical model. When using coupled models such as (1), it is good practice to work in the vicinity of a known co-existence stable fixed point, i.e a solution $X^+ = ([O_2]^+, [P]^+, [Z]^+) \neq (0,0,0)$ to Eqs. (2)-(4) that doesn't change with time and attracts nearby system trajectories. This guarantees that, when removing the advection and diffusion terms, the system will evolve to a constant state whose properties are already established (e.g. positive concentrations). The fixed points of the O₂PZ system are the states X^+ where

$$d[O_2]^+/dt = d[P]^+/dt = d[Z]^+/dt = 0 \quad (A1)$$

Since the system is nonlinear, solution of Eq. (A1) is not straightforward and approximate methods are then a good choice. Since the model will be used to study O₂ dynamics in coastal upwelling systems in the Iberian Peninsula western shelf/slope, it is logical that the model uses initial conditions that are characteristic of this region. The characteristic state $X^w = ([O_2]^w, [P]^w, [Z]^w)$ may be taken from climatological dataset, in-situ observations, remotely-sensed data, etc. as long as it is representative of the actual values of ([O₂],[P],[Z]) in that region. Regarding the position of X^w in the state space, a simple proposition is that X^w is close to a coexistence steady state X^0 . This means that, if the model is initialized at X^w it will converge to X^0 and will not evolve to an extinction state or other steady states with unrealistic or uncharacteristic values of ([O₂],[P],[Z]) for the region. This is the approach adopted here to study the fixed points and determine the values of the parameters of the system and we adopt the characteristic values shown in Table A1 for the Iberian Peninsula upwelling.

Table A1. Characteristics values of O₂, P and Z for the western Iberian Peninsula.

Variable	Value
[O ₂] ^w	0.255 mmol O L ⁻¹
[P] ^w	0.063 mmol O m ⁻³
[Z] ^w	0.017 mmol O m ⁻³

The concentration of DO is taken from the climatological mean at 12°W, 41° N and 10 m depth. The phytoplankton concentration is obtained from ocean color images of chlorophyll a in the west Iberian shelf at approximately the same position of the DO reading, after converting it to nitrogen concentration using a ratio of 1.59 between Chl a and nitrogen content (Montes et al., 2014). Finally, the zooplankton concentration is found by using a phytoplankton to zooplankton ratio of 3.6, taken from SP2015 for the case of a stable co-existence state of the nondimensional model. For some parameters we adopt the

values that are used elsewhere in the literature. To find the most adequate values of the remaining parameters, we search for the parameters that make possible the propositions above regarding the stable nature of X^w . ~~To proceed, we consider first the system obtained by setting $[Z]=0$.~~

~~Applying the fixed point condition (A1), we obtain two equations relating $[P]$ and $[O_2]$:~~

~~$$P_1([O_2]) = (m[O_2]([O_2+e_0])([O_2]+e_2))/(Ae_0e_2+(A-\delta)e_0[O_2]-\delta[O_2]^2) \quad (A2)$$~~

~~$$P_2([O_2]) = 1/\gamma(Be/([O_2]+e_1) - \sigma) \quad (A3)$$~~

~~The fixed points of the system are given by $P_1=P_2$ in the positive quadrant of the $([O_2], [P]; [Z]=0)$ plane, in addition to the extinction steady state. Explicit computation of the fixed points is not possible for the $[O_2]$ $[P]$ $[Z]$ system, but we can derive relationships of the form $[Z]=f([O_2],[P])$ that satisfy (A1) from the oxygen and phytoplankton equations, as follows:~~

~~$$Z_1([O_2],[P]) = ([O_2]+e_2)/\gamma[O_2] ((Ae_0[P])/([O_2]+e_0) - (\delta[O_2][P])/([O_2]+e_2) - m[O_2]) \quad (A4)$$~~

~~$$Z_2([O_2],[P]) = ([P]+h)/\beta[P] (B[O_2][P]/([O_2]+e_1) - \gamma[P]^2 - \sigma[P]) \quad (A5)$$~~

~~The zooplankton equation does not produce a similar relationship. Instead, analytical manipulation of it let us derive the following expression:~~

~~$$[Z]=0 \vee [P]=P_2=hM([O_2])/(1-M([O_2])), \quad (A6)$$~~

~~where $M([O_2])=\mu/\beta - ([O_2]^2+e_1^2)/\eta[O_2]^2$. The fixed points of the $[O_2]$ $[P]$ $[Z]$ system are the locii of intersection of Eqs. (A4)-(A6) in the $([O_2] > 0; [P] > 0; [Z] > 0)$ octant. Note that the terms in parenthesis in Eqs. (A4), (A5) are the equations of the oxygen-phytoplankton system. In fact, if $[Z]=0$, Eqs. (A4), (A5) reduce to Eqs. (A2), (A3), as expected.~~

There are 11 parameters that relate O_2 with phytoplankton and zooplankton. It is a considerable amount of free parameters to handle. To constrain the choice of values for this set of parameters, making it easier to tune the model, we introduce the following three assumptions, regarding the model behaviour at X^w :

1. At X^w , zooplankton growth should not be hampered by the value of $[O_2]^w$. This requires that the feeding efficiency term is at or near its maximum h .
2. At X^w , the phytoplankton growth rate should be near or at its maximum value of B .
3. At X^w , phytoplankton O_2 production rate is significantly larger than O_2 respiration rate.

These assumptions are adopted to facilitate a co-existence state at X^w , by not limiting the ability of zooplankton to feed on phytoplankton and at the same time by facilitating phytoplankton growth to feed zooplankton and to produce O_2 in a greater amount than it respire.

~~Since the position of the fixed points of the system is given by the intersections of the isoclines Z_1 , Z_2 and P_2 , they should intersect at or near $([O_2]^w; [P]^w)$ and the fixed point at the intersection should be stable. This can be achieved by changing the parameters of the system in order to move the isoclines in phase space, and at the same time check the sign of the real part of the eigenvalues of the system Jacobian matrix at the intersection to identify the stability type of the fixed point. In Fig. A1, we plot the three isoclines in the plane $v=0$ for different values of the parameters A , B and h . It shows how the isoclines change with the changing parameters. Since both Z_1 and Z_2 depend on $[Z]$, we must look at the 3D phase space to see where the isoclines intersect (Fig. A2).~~

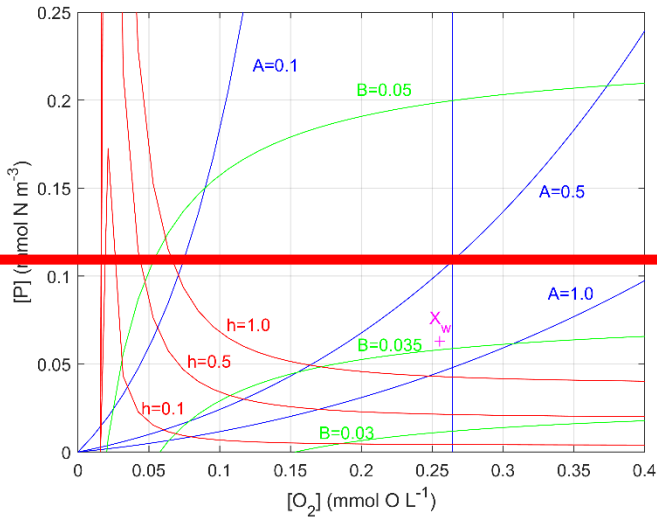


Figure A1. Isoclines of the $[O_2]$ - $[P]$ system for selected values of A , B and h . Blue: P_1 ; Green: P_2 ; Red: P_Z .

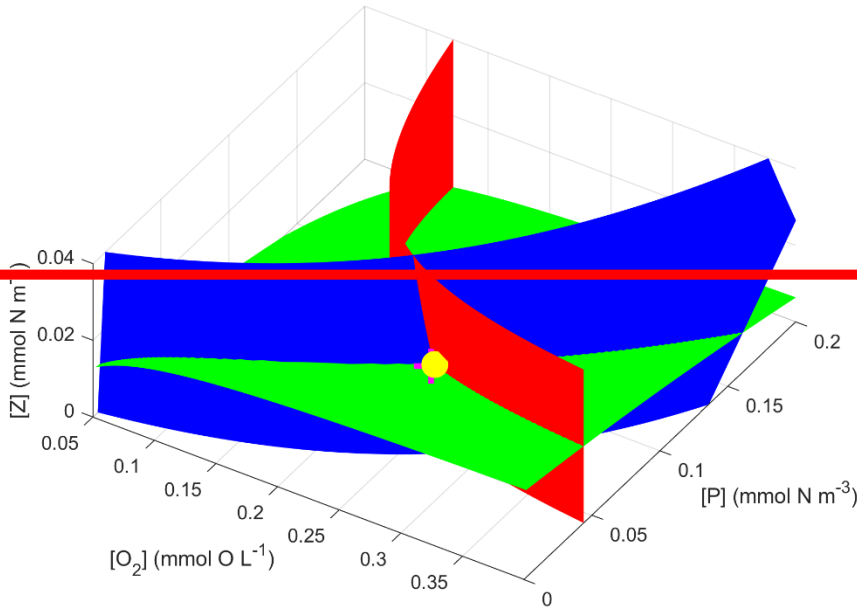


Figure A2. Isoclines of the $[O_2]$ - $[P]$ - $[Z]$ system. Blue: Z_1 ; Green: Z_2 ; Red: P_Z ; Yellow: X^0 . To build this figure, we set up a grid of $([O_2]_i, [P]_j)$; $i, j = 1, \dots, N$ values and plotted $Z_1(i; j)$ and $Z_2(i; j)$ from Eqs. (A4) and (A5). The P_Z isocline is different since it does not depend on $[Z]$, so we computed $P_Z(i) = hM(e_i) / (1 - M(e_i))$ with M defined in the text, and extended it vertically up.

To find the intersection point, that corresponds to the co-existence steady state X^0 , we computed the distance $d_{12}(i; j) = Z_2(i; j) - Z_1(i; j)$, so that the intersection $Z_2 = Z_1$ is given by $d_{12} = 0$. The zeros of d_{12} were identified approximately by choosing, for each $[O_2]_i$, the value of $[P]_j$ that minimized $d_{12}(i; j)$. To find X^0 , we used a similar procedure to find the point where this line intersects P_Z . This procedure is approximate, and its accuracy varies with N . By performing tests for several N , we found that $N = 300$ gave enough accuracy. By varying A , B and h , the intersection (X^0) can be made to approach X^w . Although other parameters may be varied instead of these three, we found that these are the ones whose variations are easier to judge in terms of displacement of the isoclines. We note that, of the three, only h is one of the "fixed" parameters that was found in the literature, but since it is quite easy to move P_Z by changing its value, we decided to use it as a tuning parameter. The result of this exercise is that the This results in a co-existence fixed point X^0 that is located near X^w , with coordinates shown in Table 2 and is a stable spiral point with eigenvalues of the Jacobian $\lambda_1 = -0.0847$ and $\lambda_{2,3} = -0.0009 \pm 0.0221i$.

Table A2. Coordinates of the co-existence fixed point X^0 .

Variable	Value
$[O_2]^0$	0.261 mmol O L ⁻¹
$[P]^0$	0.052 mmol N m ⁻³
$[Z]^0$	0.018 mmol N m ⁻³

Table A3. Parameters of the 0-D SP2015 biogeochemical model.

Parameter	Value	Units	Description
A	0.54	d ⁻¹	Environmental effects in rate of O ₂ production inside phytoplankton cells.
c_0	0.255	mmol O L ⁻¹	Half-saturation constant for O ₂ production.
δ	0.2	d ⁻¹	Maximum per capita phytoplankton respiration rate.
c_2	0.255	mmol O L ⁻¹	Half-saturation constant for O ₂ respiration by phytoplankton
ν	0.35	d ⁻¹	Maximum per capita zooplankton respiration rate.
c_3	0.255	mmol O L ⁻¹	Half-saturation constant for O ₂ respiration by zooplankton
m	0.03	d ⁻¹	Rate of oxygen loss due to natural depletion.
B	0.055	d ⁻¹	Maximum per capita phytoplankton growth rate.
c_1	0.017	mmol O L ⁻¹	Half-saturation constant for phytoplankton growth.
γ	0.1	mmol O L ⁻¹ d ⁻¹	Intensity of intra-specific competition.
β	0.9	d ⁻¹	Maximum zooplankton predation rate.
H	0.8	mmol N m ⁻³	Half-saturation constant for phytoplankton predation.
σ	0.027	d ⁻¹	Phytoplankton mortality rate.
η	0.75	-	Maximum zooplankton feeding efficiency.
c_4	0.255	mmol O L ⁻¹	Half-saturation constant for zooplankton feeding efficiency.
μ	0.025	d ⁻¹	Zooplankton mortality rate.

Appendix B. Dynamics of the ECC simulation

We analyze the dynamics of the ECC simulation in terms of turbulent energy transfers, mean and eddy-induced circulations and dominant turbulent length scales. Mean quantities refer to the along-shore average, e.g., for the cross-shore velocity u :

$$\langle u(x,z,t) \rangle = L^{-1} \int u(x,y,z,t) dy \quad (B1)$$

where L is the along-shore length of the channel. Perturbations are the departures from this mean: $u' = u - \langle u \rangle$ and $\langle u' \rangle = 0$. The mean kinetic energy transfer term is $\langle cke \rangle = -\rho_0 (\langle v_x \rangle \langle u' v' \rangle + \langle v_z \rangle \langle w' v' \rangle + \langle u_x \rangle \langle u' u' \rangle + \langle u_z \rangle \langle w' u' \rangle)$, where ρ_0 is the reference density, v and w the along-shore and vertical velocities and a subscript denotes partial differentiation. The perturbation potential energy transfer term is $\langle cpe \rangle = -g \langle w' \rho' \rangle$.

In the ECC case $\langle cpe \rangle$ remains positive, increasing after the wind intensification part of the wind cycle and decreasing when the wind relaxes (Fig. B1a), while $\langle cke \rangle$ oscillates between positive and negative values. The mechanism for $\langle cke \rangle$ growth seems to be the coalescence of disturbances into a single large eddy that is subsequently perturbed by rapidly emerging small scale patterns (Durski and Allen, 2005). Anti-correlation between $\langle cpe \rangle$ and $\langle cke \rangle$ is observable at days 35, 47, 53 and 60 (Fig. B1a), suggesting that $\langle cke \rangle$ evolution is related to nonlinear wave-wave interaction rather than to wave-mean flow interaction (Durski

and Allen, 2005). For sustained winds, like the ECC wind cycle with short wind intensification and relaxation periods, the effects of this interaction are significant since the start of the simulations (Durski et al., 2007).

Initially, the surface density peak length-scale l_e , i.e. the most energetic scale, is homogeneous, and l_e is equal to the domain length (Figure B1b).

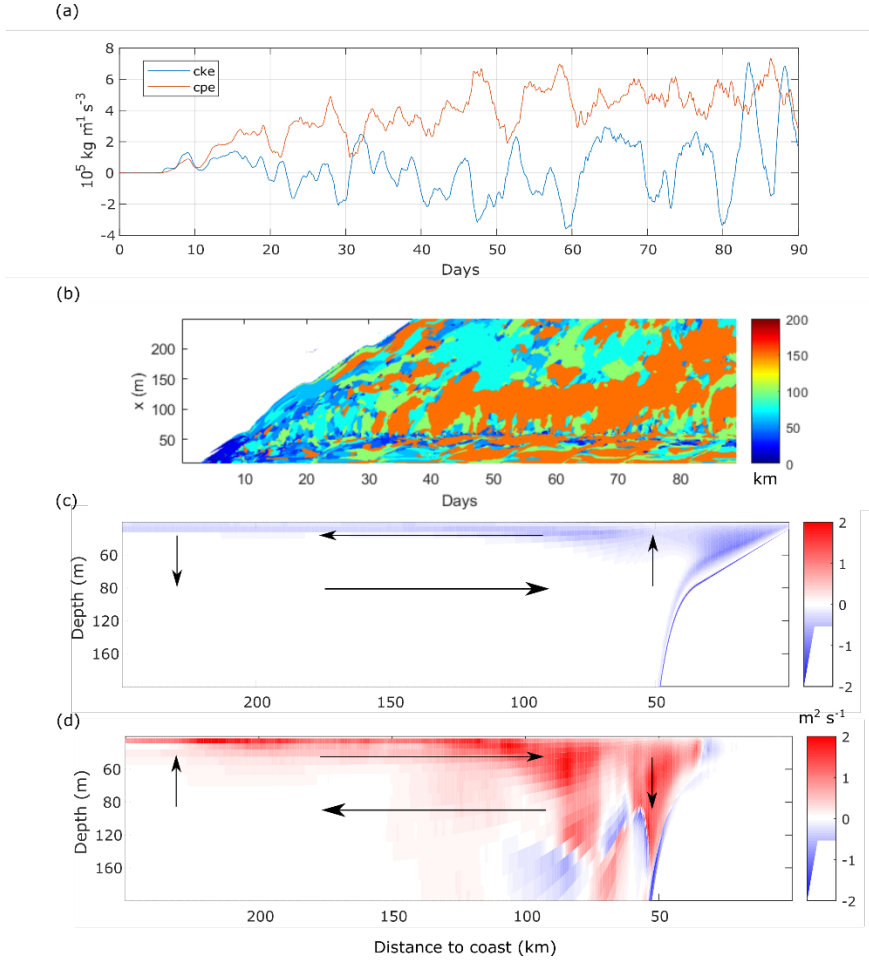


Figure B1. a) Time series of volume averaged perturbation energy source terms; cke source term (green) and cpe source term (blue); volume average in the whole domain. **b)** Peak wavelength of surface density anomaly alongshore wavenumber spectrum as a function of time and offshore distance. **c)** Mean stream-function over days 20 to 90. **d)** Eddy stream-function over days 20 to 90. Mean stratification is shown as black dash-dot contours in panels c and d. Arrows in panels c and d represent a schematic view of the circulation.

Shortly after the start, small-scale ($O(10\text{km})$) fluctuations appear close to shore, then grow in length and spread offshore. From day 20 onwards, l_e fully develops and ranges from 20 to 160 km across shore, although until day 36 there are still regions where density is rather homogeneous.

Offshore of the upwelling front (roughly from 50 km) we observe the emergence of two distinct regions in the across-shore direction: a region adjacent to the front where large scale structures are often dominant ($l_e \sim 150 - 160 \text{ km}$), and further offshore where smaller-scale structures are dominant ($l_e < 100 \text{ km}$). The cross-shore extent of the first region appears to be related to the excursions in the cke time serie (Fig. 3a), judging by the coincidence of the largest fluctuations of cke with the widest swaths of $l_e \sim 150 - 160 \text{ km}$ (days 45, 60, 68 and 80). The second region further offshore seldom exhibits $l_e > 100 \text{ km}$ as it is usually populated by filaments emerging from the front with contrasted density and by vortices resulting from the roll up of filament tips.

The wind-induced mean circulation in the x - z plane is $\Psi = -\tau/\rho_0 f$ where τ is the applied wind stress and f the Coriolis parameter. The eddy stream-function is $\psi = (\langle v'b' \rangle \langle b'_z \rangle - \lambda^2 \langle w'b' \rangle \langle b'_y \rangle) / (\lambda^2 \langle w'b' \rangle \langle b'_y \rangle + \langle b'_z \rangle)$, where b is buoyancy and $\lambda = 1000$ is a stretching constant that accounts for the large aspect ratio of oceanic flows (Nagai et al., 2015; Plumb and Ferrari, 2005).

The wind-induced mean circulation in the vertical cross-shore plane (Fig. B1c) is stronger at the surface and near the coast and weaker in the interior. A typical upwelling circulation is simulated: Ekman transport moves surface waters offshore and upwards near the coast giving rise to the mean upward tilting of the isopycnals. The eddy induced stream-function (Fig. B1d) represents the component of the flow across the mean isopycnals (Cerovečki et al., 2009; Plumb and Ferrari, 2005), opposes the mean circulation and can surpass it. In agreement with Cerovečki et al. (2009) we find that the eddy stream-function is stronger at the diabatic surface layer, in a thin layer (up to 20 m depth) with strong shoreward circulation 100 km offshore, deepening to 150 m at 75 km offshore. There is another strong eddy downwelling cell, on the shelf–slope transition, that goes down to 160 m depth.

The submesoscale and mesoscale turbulence is sustained by energy transfer from the potential energy field to the turbulent kinetic energy field, through baroclinic conversion (Durski and Allen, 2005; Marchesiello et al., 2003). In agreement with previous modelling studies (Capet et al., 2008; Durski and Allen, 2005), the global picture is thus that the intermittent wind bursts act as a recharge for the mean potential energy which is then released to eddy kinetic energy through baroclinic instability. When the wind decreases, the eddy flux induces a rapid re-stratification of the upper layer (Capet et al., 2008).

Author contributions

JHB, VR and VG design the study with input from LR, YM and PH. JHB performed the simulations. JHB, VR and VG analysed the results and prepared the draft manuscript. All authors critically reviewed, commented and prepared the final manuscript.

Acknowledgements

This work is part of the TEASAO project, funded by "IDEX attractivity chairs" program from University of Toulouse. JHB acknowledges post-doctoral fellowship financial support from the TEASAO project and CENTEC (University of Lisbon) for hosting him during his stays. VR acknowledges fruitful discussions with M. Marta-Almeida and travel support from INSU-CNRS. The MOUTON 2007 campaign was carried out as part of a SHOM (Service Hydrographique et Océanographique de la Marine) project and we acknowledge the competence and investment of the SHOM technical staff who took part in it.

References

- Adams, K. A., Barth, J. A. and Chan, F.: Temporal variability of near-bottom dissolved oxygen during upwelling off central Oregon, *Journal of Geophysical Research: Oceans*, 118(10), 4839–4854, doi:10.1002/jgrc.20361, 2013.
- Alvarez-Salgado, X. A., Rosón, G., Pérez, F. F. and Pazos, Y.: Hydrographic variability off the Rías Baixas (NW Spain) during the upwelling season, *Journal of Geophysical Research*, 98(C8), 14447, doi:10.1029/93JC00458, 1993.
- Álvarez-Salgado, X.A., Nieto-Cid, M., Álvarez, M., Pérez, F.F., Morin, P., Mercier, H.: New insights on the mineralization of dissolved organic matter in central, intermediate, and deep water masses of the northeast North Atlantic. *Limnol. Oceanogr.* 58, 681–696. doi.org/10.4319/lo.2013.58.2.0681, 2013.
- Behrenfeld, M. J., Halsey Kimberly H and Milligan Allen J: Evolved physiological responses of phytoplankton to their integrated growth environment, *Philosophical Transactions of the Royal Society B: Biological Sciences*, 363(1504), 2687–2703, doi:10.1098/rstb.2008.0019, 2008.
- Bettencourt, J. H., López, C., Hernández-García, E., Montes, I., Sudre, J., Dewitte, B., Paulmier, A. and Garçon, V.: Boundaries of the Peruvian oxygen minimum zone shaped by coherent mesoscale dynamics, *Nature Geoscience*, 8(12), 937–940, doi:10.1038/ngeo2570, 2015.

- Bettencourt, J. H., Rossi, V., Hernández-García, E., Marta-Almeida, M. and López, C.: Characterization of the Structure and Cross-Shore Transport Properties of a Coastal Upwelling Filament Using Three-Dimensional Finite-Size Lyapunov Exponents, *Journal of Geophysical Research: Oceans*, 122(9), 7433–7448, doi:10.1002/2017JC012700, 2017.
- Boyer, T. P., Antonov, J. I., Baranova, O. K., Coleman, C., Garcia, H. E., Grodsky, A., Johnson, D. R., Locarnini, R. A., Mishonov, A. V., O'Brien, T. D. and others: *World Ocean Database 2013.*, 2013.
- Breitburg, D., Levin, L. A., Oschlies, A., Grégoire, M., Chavez, F. P., Conley, D. J., Garçon, V., Gilbert, D., Gutiérrez, D., Isensee, K., Jacinto, G. S., Limburg, K. E., Montes, I., Naqvi, S. W. A., Pitcher, G. C., Rabalais, N. N., Roman, M. R., Rose, K. A., Seibel, B. A., Telszewski, M., Yasuhara, M. and Zhang, J.: Declining Oxygen in the Global Ocean and Coastal Waters, *Science*, 359(6371), eaam7240, doi:10.1126/science.aam7240, 2018.
- Breitburg, D. L., Loher, T., Pacey, C. A. and Gerstein, A.: Varying Effects of Low Dissolved Oxygen on Trophic Interactions in an Estuarine Food Web, *Ecological Monographs*, 67(4), 489–507, doi:10.2307/2963467, 1997.
- Capet, X., McWilliams, J., Molemaker, M. and Shchepetkin, A.: Mesoscale to Submesoscale Transition in the California Current System. Part I: Flow Structure, Eddy Flux, and Observational Tests, *Journal of Physical Oceanography*, 38(1), 29–43, 2008.
- Capet, A., Meysman, F.J.R., Akoumianaki, I., Soetaert, K., Grégoire, M.: Integrating sediment biogeochemistry into 3D oceanic models: A study of benthic-pelagic coupling in the Black Sea. *Ocean Modelling* 101, 83–100. doi.org/10.1016/j.ocemod.2016.03.006, 2016.
- Castaing, B., Gagne, Y. and Hopfinger, E. J.: Velocity Probability Density Functions of High Reynolds Number Turbulence, *Physica D: Nonlinear Phenomena*, 46(2), 177–200, doi:10.1016/0167-2789(90)90035-N, 1990.
- Castro, C.G., Nieto-Cid, M., Álvarez-Salgado, X.A., Pérez, F.F.: Local remineralization patterns in the mesopelagic zone of the Eastern North Atlantic, off the NW Iberian Peninsula. *Deep Sea Research Part I: Oceanographic Research Papers* 53, 1925–1940. doi.org/10.1016/j.dsr.2006.09.002, 2006.
- Cerovečki, I., Plumb, R. A. and Heres, W.: Eddy Transport and Mixing in a Wind- and Buoyancy-Driven Jet on the Sphere, *Journal of Physical Oceanography*, 39(5), 1133–1149, doi:10.1175/2008JPO3596.1, 2009.
- Chaigneau, A., Eldin, G. and Dewitte, B.: Eddy Activity in the Four Major Upwelling Systems from Satellite Altimetry (1992–2007), *Progress in Oceanography*, 83(1), 117–123, doi:10.1016/j.pocean.2009.07.012, 2009.
- Charney, J. G.: Geostrophic Turbulence, *Journal of the Atmospheric Sciences*, 28(6), 1087–1095, doi:10.1175/1520-0469(1971)028<1087:GT>2.0.CO;2, 1971.
- Combes, V., Chenillat, F., Lorenzo, E. D., Rivière, P., Ohman, M. D. and Bograd, S. J.: Cross-Shore Transport Variability in the California Current: Ekman Upwelling vs. Eddy Dynamics, *Progress in Oceanography*, 109, 78–89, doi:10.1016/j.pocean.2012.10.001, 2013.
- Debreu, L., Marchesiello, P., Penven, P. and Cambon, G.: Two-Way Nesting in Split-Explicit Ocean Models: Algorithms, Implementation and Validation, *Ocean Modelling*, 49, 1–21, 2012.
- Diaz, R. J. and Rosenberg, R.: Spreading Dead Zones and Consequences for Marine Ecosystems, *Science*, 321(5891), 926–929, doi:10.1126/science.1156401, 2008.
- Durski, S. M. and Allen, J. S.: Finite-Amplitude Evolution of Instabilities Associated with the Coastal Upwelling Front, *Journal of Physical Oceanography*, 35(9), 1606–1628, doi:10.1175/JPO2762.1, 2005.
- Durski, S. M., Allen, J. S., Egbert, G. D. and Samelson, R. M.: Scale Evolution of Finite-Amplitude Instabilities on a Coastal Upwelling Front, *Journal of Physical Oceanography*, 37(4), 837–854, doi:10.1175/JPO2994.1, 2007.
- Feng, Y., DiMarco, S. F. and Jackson, G. A.: Relative role of wind forcing and riverine nutrient input on the extent of hypoxia in the northern Gulf of Mexico, *Geophysical Research Letters*, 39(9), n/a-n/a, doi:10.1029/2012GL051192, 2012.
- Forrest, D. R., Hetland, R. D. and DiMarco, S. F.: Multivariable statistical regression models of the areal extent of hypoxia over the Texas–Louisiana continental shelf, *Environ. Res. Lett.*, 6(4), 045002, doi:10.1088/1748-9326/6/4/045002, 2011.
- Gilly, W. F., Beman, J. M., Litvin, S. Y. and Robison, B. H.: Oceanographic and Biological Effects of Shoaling of the Oxygen Minimum Zone, *Annual Review of Marine Science*, 5(1), 393–420, doi:10.1146/annurev-marine-120710-100849, 2013.

- Gomes, H. do R., Goes, J. I., Matondkar, S. G. P., Buskey, E. J., Basu, S., Parab, S. and Thoppil, P.: Massive outbreaks of *Noctiluca scintillans* blooms in the Arabian Sea due to spread of hypoxia, *Nature Communications*, 5, 4862, doi:10.1038/ncomms5862, 2014.
- Grantham, B. A., Chan, F., Nielsen, K. J., Fox, D. S., Barth, J. A., Huyer, A., Lubchenco, J. and Menge, B. A.: Upwelling-Driven Nearshore Hypoxia Signals Ecosystem and Oceanographic Changes in the Northeast Pacific, *Nature*, 429(6993), nature02605, doi:10.1038/nature02605, 2004.
- Gregg, W. W., Rousseaux, C. S. and Franz, B. A.: Global trends in ocean phytoplankton: a new assessment using revised ocean colour data, *Remote Sensing Letters*, 8(12), 1102–1111, doi:10.1080/2150704X.2017.1354263, 2017.
- Gruber, N., Lachkar, Z., Frenzel, H., Marchesiello, P., Munnich, M., McWilliams, J., Nagai, T. and Plattner, G.: Eddy-Induced Reduction of Biological Production in Eastern Boundary Upwelling Systems, *Nature Geoscience*, 4(11), 787–792, doi:10.1038/NGEO1273, 2011.
- Gutknecht, E., Dadou, I., Le Vu, B., Cambon, G., Sudre, J., Garçon, V., Machu, E., Rixen, T., Kock, A., Flohr, A., Paulmier, A. and Lavik, G.: Coupled Physical/Biogeochemical Modeling Including O₂-Dependent Processes in the Eastern Boundary Upwelling Systems: Application in the Benguela, *Biogeosciences*, 10(6), 3559–3591, doi:10.5194/bg-10-3559-2013, 2013.
- Hales, B., Karp-Boss, L., Perlin, A. and Wheeler, P. A.: Oxygen Production and Carbon Sequestration in an Upwelling Coastal Margin, *Global Biogeochemical Cycles*, 20(3), GB3001, doi:10.1029/2005GB002517, 2006.
- Harris, G. P.: *Phytoplankton Ecology*, Springer Netherlands, Dordrecht., 1986.
- Head, E. J. H. and Pepin, P.: Spatial and inter-decadal variability in plankton abundance and composition in the Northwest Atlantic (1958–2006), *J Plankton Res*, 32(12), 1633–1648, doi:10.1093/plankt/fbq090, 2010.
- Hernández-Carrasco, I., Rossi, V., Hernández-García, E., Garçon, V. and López, C.: The Reduction of Plankton Biomass Induced by Mesoscale Stirring: A Modeling Study in the Benguela Upwelling, *Deep Sea Research Part I: Oceanographic Research Papers*, 83(Supplement C), 65–80, doi:10.1016/j.dsr.2013.09.003, 2014.
- Laffoley, D. and Baxter, J., 2019, *Ocean deoxygenation : everyone's problem : causes, impacts, consequences and solutions*, IUCN Report, Gland, Switzerland, 562 pages, doi.org/10.2305/IUCN.CH.2019.13.en
- Large, W. G., McWilliams, J. C. and Doney, S. C.: Oceanic Vertical Mixing: A Review and a Model with a Nonlocal Boundary Layer Parameterization, *Reviews of Geophysics*, 32(4), 363–403, 1994.
- ~~Levin, L. A.: Manifestation, Drivers, and Emergence of Open Ocean Deoxygenation, *Annual Review of Marine Science*, doi:10.1146/annurev-marine-121916-063359, 2018.~~
- López-Sandoval, D. C., Rodríguez-Ramos, T., Cermeño, P., Sobrino, C. and Marañón, E.: Photosynthesis and respiration in marine phytoplankton: Relationship with cell size, taxonomic affiliation, and growth phase, *Journal of Experimental Marine Biology and Ecology*, 457, 151–159, doi:10.1016/j.jembe.2014.04.013, 2014.
- Lovecchio, E., Gruber, N., Münnich, M. and Lachkar, Z.: On the long-range offshore transport of organic carbon from the Canary Upwelling System to the open North Atlantic, *Biogeosciences*, 14(13), 3337–3369, doi:10.5194/bg-14-3337-2017, 2017.
- Mackey, K. R. M., Paytan, A., Grossman, A. R. and Bailey, S.: A photosynthetic strategy for coping in a high-light, low-nutrient environment, *Limnology and Oceanography*, 53(3), 900–913, doi:10.4319/lo.2008.53.3.0900, 2008.
- Marchesiello, P., McWilliams, J. C. and Shchepetkin, A.: Equilibrium Structure and Dynamics of the California Current System, *J. Phys. Oceanogr.*, 33(4), 753–783, doi:10.1175/1520-0485(2003)33<753:ESADOT>2.0.CO;2, 2003.
- Marta-Almeida, M., Reboreda, R., Rocha, C., Dubert, J., Nolasco, R., Cordeiro, N., Luna, T., Rocha, A., e Silva, J. D. L., Queiroga, H., Peliz, A. and Ruiz-Villarreal, M.: Towards Operational Modeling and Forecasting of the Iberian Shelves Ecosystem, *PLOS ONE*, 7(5), e37343, doi:10.1371/journal.pone.0037343, 2012.
- McClatchie, S., Goericke, R., Cosgrove, R., Auad, G., and Vetter, R.: Oxygen in the Southern California Bight: Multidecadal trends and implications for demersal fisheries, *Geophys. Res. Lett.*, 37, L19602, doi:10.1029/2010GL044497, 2010.

- Miranda, P. M. A., Alves, J. M. R. and Serra, N.: Climate change and upwelling: response of Iberian upwelling to atmospheric forcing in a regional climate scenario, *Clim Dyn*, 40(11–12), 2813–2824, doi:10.1007/s00382-012-1442-9, 2013.
- Moncoiffé, G., Alvarez-Salgado, X. A., Figueiras, F. G. and Savidge, G.: Seasonal and short-time-scale dynamics of microplankton community production and respiration in an inshore upwelling system, *Marine Ecology Progress Series*, 196, 111–126, doi:10.3354/meps196111, 2000.
- Montes, I., Dewitte, B., Gutknecht, E., Paulmier, A., Dadou, I., Oschlies, A. and Garçon, V.: High-Resolution Modeling of the Eastern Tropical Pacific Oxygen Minimum Zone: Sensitivity to the Tropical Oceanic Circulation, *Journal of Geophysical Research: Oceans*, n/a–n/a, doi:10.1002/2014JC009858, 2014.
- Nagai, T., Gruber, N., Frenzel, H., Lachkar, Z., McWilliams, J. C. and Plattner, G.-K.: Dominant Role of Eddies and Filaments in the Offshore Transport of Carbon and Nutrients in the California Current System, *Journal of Geophysical Research: Oceans*, 120(8), 5318–5341, doi:10.1002/2015JC010889, 2015.
- Paulmier, A. and Ruiz-Pino, D.: Oxygen Minimum Zones (OMZs) in the Modern Ocean, *Progress in Oceanography*, 80(3), 113–128, 2009.
- [Pérez, F.F., Castro, C.G., Álvarez-Salgado, X.A., Ríos, A.F.: Coupling between the Iberian basin — scale circulation and the Portugal boundary current system: a chemical study. *Deep Sea Research Part I: Oceanographic Research Papers* 48, 1519–1533. doi.org/10.1016/S0967-0637\(00\)00101-1, 2001.](https://doi.org/10.1016/S0967-0637(00)00101-1)
- Petrovskii, S., Sekerci, Y. and Venturino, E.: Regime shifts and ecological catastrophes in a model of plankton-oxygen dynamics under the climate change, *Journal of Theoretical Biology*, 424, 91–109, doi:10.1016/j.jtbi.2017.04.018, 2017.
- Plumb, R. A. and Ferrari, R.: Transformed Eulerian-Mean Theory. Part I: Nonquasigeostrophic Theory for Eddies on a Zonal-Mean Flow, *Journal of Physical Oceanography*, 35(2), 165–174, doi:10.1175/JPO-2669.1, 2005.
- Reboreda, R., Cordeiro, N. G. F., Nolasco, R., Castro, C. G., Álvarez-Salgado, X. A., Queiroga, H. and Dubert, J.: Modeling the Seasonal and Interannual Variability (2001–2010) of Chlorophyll-a in the Iberian Margin, *Journal of Sea Research*, 93, 133–149, doi:10.1016/j.seares.2014.04.003, 2014.
- Reboreda, R., Castro, C. G., Álvarez-Salgado, X. A., Nolasco, R., Cordeiro, N. G. F., Queiroga, H. and Dubert, J.: Oxygen in the Iberian Margin: A Modeling Study, *Progress in Oceanography*, 131, 1–20, doi:10.1016/j.pocean.2014.09.005, 2015.
- Renault, L., Deutsch, C., McWilliams, J. C., Frenzel, H., Liang, J.-H. and Colas, F.: Partial Decoupling of Primary Productivity from Upwelling in the California Current System, *Nature Geoscience*, 9(7), 505–508, doi:10.1038/ngeo2722, 2016.
- Roegner, G. C., Needoba, J. A. and Baptista, A. M.: Coastal Upwelling Supplies Oxygen-Depleted Water to the Columbia River Estuary, *PLOS ONE*, 6(4), e18672, doi:10.1371/journal.pone.0018672, 2011.
- Rossi, V., Morel, Y. and Garçon, V.: Effect of the Wind on the Shelf Dynamics: Formation of a Secondary Upwelling along the Continental Margin, *Ocean Modelling*, 31 (3–4), 51–79, 2010.
- Rossi, V., Garçon, V., Tassel, J., Romagnan, J.-B., Stemmann, L., Jourdin, F., Morin, P. and Morel, Y.: Cross-Shelf Variability in the Iberian Peninsula Upwelling System: Impact of a Mesoscale Filament, *Continental Shelf Research*, 59, 97–114, 2013.
- Rykaczewski, R. R., Dunne, J. P., Sydeman, W. J., García-Reyes, M., Black, B. A. and Bograd, S. J.: Poleward displacement of coastal upwelling-favorable winds in the ocean's eastern boundary currents through the 21st century, *Geophysical Research Letters*, 42(15), 6424–6431, doi:10.1002/2015GL064694, 2015.
- [Sarthou, G., Timmermans, K.R., Blain, S., Tréguer, P.: Growth physiology and fate of diatoms in the ocean: a review. *Journal of Sea Research, Iron Resources and Oceanic Nutrients - Advancement of Global Environmental Simulations* 53, 25–42. doi.org/10.1016/j.seares.2004.01.007, 2005.](https://doi.org/10.1016/j.seares.2004.01.007)
- Sekerci, Y. and Petrovskii, S.: Mathematical Modelling of Plankton–Oxygen Dynamics under the Climate Change, *Bulletin of mathematical biology*, 77(12), 2325–2353, 2015.
- Shchepetkin, A. F.: An Adaptive, Courant-Number-Dependent Implicit Scheme for Vertical Advection in Oceanic Modeling, *Ocean Modelling*, 91, 38–69, doi:10.1016/j.ocemod.2015.03.006, 2015.

- Shchepetkin, A. F. and McWilliams, J. C.: The Regional Oceanic Modeling System (ROMS): A Split-Explicit, Free-Surface, Topography-Following-Coordinate Oceanic Model, *Ocean Modelling*, 9(4), 347–404, doi:10.1016/j.ocemod.2004.08.002, 2005.
- Siedlecki, S. A., Banas, N. S., Davis, K. A., Giddings, S., Hickey, B. M., MacCready, P., Connolly, T. and Geier, S.: Seasonal and interannual oxygen variability on the Washington and Oregon continental shelves, *Journal of Geophysical Research: Oceans*, 120(2), 608–633, doi:10.1002/2014JC010254, 2015.
- Sousa, M. C., deCastro, M., Alvarez, I., Gomez-Gesteira, M. and Dias, J. M.: Why coastal upwelling is expected to increase along the western Iberian Peninsula over the next century?, *Science of The Total Environment*, 592, 243–251, doi:10.1016/j.scitotenv.2017.03.046, 2017.
- [Stramma, L., Johnson, G.C., Sprintall, J., Mohrholz, V.: Expanding Oxygen-Minimum Zones in the Tropical Oceans. *Science* 320, 655–658. doi.org/10.1126/science.1153847, 2008.](#)
- [Sydeman, W.J., García-Reyes, M., Schoeman, D.S., Rykaczewski, R.R., Thompson, S.A., Black, B.A., Bograd, S.J.: Climate change and wind intensification in coastal upwelling ecosystems. *Science* 345, 77–80. doi.org/10.1126/science.1251635, 2014.](#)
- Torres, R., Barton, E. D., Miller, P. and Fanjul, E.: Spatial patterns of wind and sea surface temperature in the Galician upwelling region, *Journal of Geophysical Research: Oceans*, 108(C4), doi:10.1029/2002JC001361, 2003.
- Vaquier-Sunyer, R. and Duarte, C.: Thresholds of Hypoxia for Marine Biodiversity, *Proceedings of the National Academy of Sciences of the United States of America*, 105(40), 15452–15457, doi:10.1073/pnas.0803833105, 2008.
- Vergara, O., Dewitte, B., Montes, I., Garçon, V., Ramos, M., Paulmier, A. and Pizarro, O.: Seasonal Variability of the Oxygen Minimum Zone off Peru in a High-Resolution Regional Coupled Model, *Biogeosciences*, 13(15), 4389–4410, doi:10.5194/bg-13-4389-2016, 2016.
- Wang, D., Gouhier, T. C., Menge, B. A. and Ganguly, A. R.: Intensification and spatial homogenization of coastal upwelling under climate change, *Nature*, 518(7539), 390–394, doi:10.1038/nature14235, 2015.
- [Wanninkhof, R.: Relationship between wind speed and gas exchange over the ocean, *Journal of Geophysical Research*, 97\(C5\), 7373, doi:10.1029/92JC00188, 1992.](#)
- Wooster, W. S., Bakun, A. and McLain, D. R.: SEASONAL UPWELLING CYCLE ALONG THE EASTERN BOUNDARY OF THE NORTH ATLANTIC., *J Mar Res*, 34(2), 131–141, 1976.
- Wright, J. J., Konwar, K. M. and Hallam, S. J.: Microbial Ecology of Expanding Oxygen Minimum Zones, *Nature Reviews Microbiology*, doi:10.1038/nrmicro2778, 2012.
- Zehr, J. P. and Kudela, R. M.: Photosynthesis in the Open Ocean, *Science*, 326(5955), 945–946, doi:10.1126/science.1181277, 2009.
- Zhai, L., Platt, T., Tang, C., Sathyendranath, S. and Walne, A.: The response of phytoplankton to climate variability associated with the North Atlantic Oscillation, *Deep Sea Research Part II: Topical Studies in Oceanography*, 93, 159–168, doi:10.1016/j.dsr2.2013.04.009, 2013.
- Zhang, H., Cheng, W., Chen, Y., Yu, L. and Gong, W.: Controls on the interannual variability of hypoxia in a subtropical embayment and its adjacent waters in the Guangdong coastal upwelling system, northern South China Sea, *Ocean Dynamics*, 68(8), 923–938, doi:10.1007/s10236-018-1168-2, 2018.

influences the oxygen cycle, related to processes in the benthic layers, and on remineralization processes that influence the oxygen cycle, and that are not referred to.

Authors: *We are grateful to the referee for bringing to our attention to this interesting body of previous research. We indeed referred to Rossi et al.'s articles since the dataset of this specific campaign was used to tune our model (e.g. nitrate/temperature relationship) and to compare its simulated outputs to in-situ observations. Note also that some of the authors suggested by referee 2 were already cited in our original manuscript (e.g. Alvarez-Salgado et al. 1993; Reboreda et al. 2014; 2015). Following his/her suggestions, we have now included additional references to Pérez et al (2001), Castro et al (2006) and Alvarez-Salgado et al. (2013) as follows:*

“During the upwelling season, hydrographic and biogeochemical variability is primarily determined by the wind forcing that controls the inflow of offshore deep water masses onto the shelf (Alvarez-Salgado et al., 1993). DO levels in these subsurface waters are thought to diminish during the upwelling season due to strong remineralization of sinking organic matter as well as to mixing with poorly-ventilated waters of subtropical origins (Castro et al., 2006). Overall, DO appears to partly control the remineralization of dissolved organic carbon in the IPUS and more generally in key water masses of the North Atlantic (Alvarez-Salgado et al. 2013).”

“These structures have a strong influence on the cross-shore transport and on the vertical redistribution of biogeochemical tracers (Bettencourt et al., 2017; Combes et al., 2013; Gruber et al., 2011; Hernández-Carrasco et al., 2014; Nagai et al., 2015; Renault et al., 2016; Rossi et al., 2013). In the Iberian basin, the Eastern North Atlantic Central Water (ENACW) mass of subtropical origin, whose archetypal concentrations of DO are initially low, would be ventilated by eddy-induced mixing with more oxygenated ENACW of subpolar origin (Pérez et al., 2001).”

Concerning the second part of this comment, we agree with referee 2 that our O2PZ model disregards, as a result of its low complexity, some oceanographic processes that influence oxygen cycling over the shelf, such as complex processes occurring within the benthic boundary layers or into the upper sedimentary layers (i.e. the so-called benthic-pelagic coupling). We now acknowledged this limitation of our idealized modeling approach in the revised Discussion and Conclusions section (Section 4, 1st paragraph):

“We built a coupled physical-biogeochemical model of an idealized seasonal coastal upwelling to study the effect of the upwelling season length and phytoplankton community structure on dissolved oxygen inventory. The low-complexity O₂PZ model accounts for oxygen production by photosynthesis and consumption by both respiration and remineralization but its simplicity does not allow to include other oceanographic processes that could influence oxygen cycling over shallow shelves, such as for instance the complex benthic-pelagic coupled processes (Capet et al., 2016).”

Ref. #2: *3 - Lines 62-64 need a reference that support those statement.*

Authors: We have added appropriate references to support those statements.

“Moreover, diatoms growth is thought to be positively correlated with the upwelling-driven nitrate inputs (Sarhou et al., 2005); in contrast, the growth of other planktonic groups can be insensitive to and even limited by newly-upwelled nitrates (Mahaffey, 2005), especially when colimitation prevails or in the absence of necessary micro-nutrients.”

Ref. #2: *4 - Is the implementation of the Biogeochemical (BGQ) module done in CROCO model, or was implemented from scratch?. This is not clear in the ms. In that case, justify why none of the other BGQ modules was not used.*

Authors: *Our low-complexity model centered on oxygen was implemented from scratch in the CROCO model, i.e. it was hard-coded into the CROCO model following, as a template, one of the already-embedded BGQ modules. The O2PZ model was retained instead of other BGQ models available in CROCO because of its low complexity (only 3 equations) resulting in fast and efficient computing, hence allowing running/analyzing multiple simulations while considering the role of high-resolution dynamics (e.g. submesoscale) for oxygen cycling. It has been specified in the manuscript (beginning of sect. 2.1):*

“The low-complexity O₂PZ model was directly implemented into the CROCO model following one of the already-embedded biogeochemical modules; it allows maintaining the full capabilities and versatility of this community code while gaining in computing efficiency (allowing extensive sensitivity studies and the consideration of submesoscale dynamics in oxygen cycling) as compared to the more complex biogeochemical modules already available within CROCO.”

Ref. #2: *4- Is not clear the interaction with the atmosphere in the BGQ module, concerning O₂ atmosphere - ocean exchange.*

Authors: *The air-sea fluxes of DO follow the formulation of Wanninkhof (1992). The flux is $Va * ([O_2] - [O_2]_{sat})$, where Va is the gas piston velocity, $[O_2]$ is the DO concentration at the water surface (the first sigma level below the surface) and $[O_2]_{sat}$ is the O₂ solubility in seawater. Please, see Equation 1 and the description of the DO gas exchange in the revised version of the manuscript (end of 2nd paragraph in page 4):*

“On top of the oxygen that is produced and consumed within marine ecosystems, a considerable part of dissolved oxygen eventually becomes gaseous and is then exchanged at the ocean-atmosphere interface, contributing to the estimations that more than one half of atmospheric oxygen is produced in the ocean (Harris, 1986). The remaining term of Eq. (2) is the air-sea flux of O₂, which is the product of the gas transfer velocity Va , that depends on the square of the wind speed and on the Schmidt number (Wanninkhof, 1992), with the difference of the oceanic DO concentration and the solubility of O₂ in seawater.”

Ref. #2: *5- Laplacian mixing along sigma surfaces tends to generate spurious currents. Why you did not use (ro- tated) mixing along Geopotential?*

Authors: *The reason for not using mixing along Geopotentials was that this option is computationally heavier than Laplacian mixing along sigma surfaces, while their methodological biases are similar. We retained the option that resulted in a faster code without compromising the quality of our analyses.*

Ref. #2: *6 - Is the wind only alongshore?, please specify. (l 109).*

Authors: *Yes. In our idealized setting the wind is only alongshore. Given the idealization level, we didn't see the need to include an across-shore wind component. We modified the text above Table 1 to make this explicit:*

“The cross-shore wind component is zero in all cases.”

Ref. #2: *7 - It should be clearer to the reader why nutrients are not introduced specifically, and what is the advantage of doing it in an O2PZ model instead of O2NPZ?*

Authors: *The addition of a nutrient compartment to the O2PZ model would make it computationally heavier and we wanted to keep the calculations as simple and as fast as possible. Thus, given that the original formulation of the O2PZ model didn't have nutrient limitation mechanism, which is important for upwelling regions such as the IPUS. As density and nitrate are closely related, especially in upwelling regions, we came up with a relatively simple way to include this nutrient limitation effect in our oxygen centered model. Please, see the revised text in the last paragraph of page 4:*

“This term [I(N)] is included here to circumvent the absence of nutrient limitation in the original O₂PZ model of SP2015. We chose to add a parametrization instead of a new equation for the nutrients because this last option would necessarily increase the complexity of the model.”

Ref. #2: *8 - The 12m/s wind pulses although exist in particular years (like the MOUTON campaign) are too high and unrealistic for the Western Iberia region. Justify better why such high values. Some sensitivity studies was done to this value?*

Authors: *Our choice of the wind pulse was based on forcing the model with a wind whose magnitude is comparable (i.e. the same order of magnitude, bearing in mind that our configuration is highly idealized) to the one observed during the MOUTON campaign. We also retained the highest magnitude (rather than the mean or lowest) because it stimulates the quickest and clearest formation of the unstable upwelling front. Note however that preliminary analyses were carried out to test several wind speeds (not shown); we found that the model responses were qualitatively similar, provided that the magnitude used is above a certain threshold, ensuring the development of upwelling (e.g. isopycnal outcropping and subsequent front destabilization). Given those results, we decided to use the wind speed that represented best the MOUTON campaign forcing conditions. We have clarified our rationale behind these choices in sect. 2.2 of the revised manuscript:*

“The cross-shore wind component is zero in all cases. Despite the fact that “true” wind patterns observed over Western Iberia are undoubtedly more variable (both in terms of direction and magnitude) than our idealized forcing inspired from a specific campaign, it provides the quickest development of a clear upwelling front generating small-scale instabilities. Note that sensitivity tests were performed (not shown) and revealed that the model responses are qualitatively similar among different wind strengths, given that the magnitude is high enough to ensure the development of the unstable upwelling front.”

Ref. #2: *9- I don't understand why in the initial vertical profile, (Fig 3a) the O2 drops to zero when in reality the O2 at 300m is closer to 230 mmol O / m³. The range of values in the region above central waters is 220-290 mmol O / m³.*

Authors: *The drop in O₂ levels is a consequence of our very idealized setting. Indeed, as the referee rightly points out, O₂ levels in the region at 300 meters are higher. However, in our highly idealized setting, we do not have subsurface O₂ inputs due to the periodic boundary conditions at the North and South boundaries. Since in the O₂PZ model, the only O₂ source is photosynthesis,*

that is zero below the euphotic zone, without the subsurface O₂ inputs, the subsurface O₂ becomes depleted by respiration and remineralization. Note that this point (absence of subsurface O₂ input) was already reported as an important point of discussion that we clearly identified as key for future work (please see sect. 4).

Ref. #2: *10 - Claim that figure 4 represents a validation seems too optimistic to me. I can't understand what the red dot represents in the figures.*

Authors: *Please, see the reply to point 11 below. The red dots are used to mark the position of the barycenter, i.e. the average values of the data for each quantity represented in the scatter plots, i.e. the x-coordinate of the red dot in figure 4a is the averaged density and the y-coordinate is the mean [O₂].*

Ref. #2: *11 - Using logarithms in Chl_a completely distorts the comparison, because the observations are showing values of 0-10 mg Chl_a.m⁻³ between isopycn 26-27 as the model rarely goes beyond 1 (at isopycn 27). Similar comment arises for O₂. If you claim those results are validated, then, any result is validated. If you insist in keeping this part as it is, I suggest that you remove the word validation, perhaps use 'qualitative comparison'.*

Authors: *We agree that the use of logarithmic scales provides mainly a qualitative comparison between model results and observations; note however that Chl_a concentrations are commonly plotted using logarithmic scales as values often span several order of magnitude, as is the case here. Nevertheless, we have modified the text to make this clear, removing all references to validation. Please, see the revised text of the last paragraph of section 2.*

"We compared the full ranges of densities ρ , DO concentrations [O₂], and chlorophyll-a concentrations [Chl-a] of the reference simulation to all compiled measurements collected during the MOUTON campaign. Given the low-complexity of the biogeochemical model and the highly idealized physical setting, a fully quantitative comparison is out of scope, however we confirm that the coupled model reproduces qualitatively well the ρ -[O₂] and ρ -[Chl-a] relationships obtained from in-situ observations."

Ref. #2: *12-Figure 5, I can understand the effect of upwelling at x= 40km that is related to shelf upwelling, but how do you interpret the dome at 60-70 km (approximately)? To use the references (1 200-204) to validate the averages of O₂ seems to me to be an over-optimistic approach. Again you can say that it is a simplified and idealized model, but do not try to convince the reader that it is validated, because readers with observational background would hardly understand it.*

Authors: *We believe the dome at 60-70 km is caused by the downwelling signal induced by the eddy induced circulation. More specifically, this downwelling divides the region of recently upwelled low DO waters into (i) the inshore low DO region (within 50 km from the shores) and (ii) the dome located at 60 – 70 km, slightly off the shelf edge. We have modified the text to highlight that our results are similar in a qualitative sense. The revised text (1st paragraph of section 3.1) now reads:*

*"In a qualitative sense our idealized model results are similar to more realistic model studies such as , Gutknecht *et al.* (2013) which in their modelling study of the Benguela upwelling region found a low [O₂] plume for the climatological month of December at the shelf edge, and to observational studies such as Hales *et al.* (2006), which for the Oregon coast, measured [O₂]*

of 70-110 mmol m⁻³ in upwelled water at the shelf break, about 200 mmol m⁻³ less than at the surface, which is the same range of the vertical gradient simulated here.”

Ref. #2: *13- Lines 210 - 215 seem more like a discussion, and their presence is not understood there.*

Authors: *Lines 210-215 provide a necessary, yet short, physical description of the simulation dynamics. It is needed to put the average DO distribution in the context of upwelling dynamics (at very first order, any oceanic tracer is influenced by the ocean circulation). Particularly, we felt that a discussion of the mean and the eddy-induced circulation was required to better explain the patterns of nearshore DO seen in Figure 5 (see also the first part of our reply to point 12: the “dome” is well explained by the eddy induced circulation which has been described just before).*